Inelastic lateral and seismic behaviour of concrete-filled steel tubular pile foundations

Serras, Dionisios N.; Panagaki, Stamatia D.; Skalomenos, Konstantinos A.; Hatzigeorgiou, George D.

DOI:
10.1016/j.soildyn.2021.106657

INELASTIC LATERAL AND SEISMIC BEHAVIOUR OF CONCRETE-FILLED STEEL TUBULAR PILE FOUNDATIONS

Dionisios N. Serras[1], Stamatia D. Panagaki[1,2], Konstantinos A. Skalomenos[3], George D. Hatzigeorgiou[1]

[1]School of Science and Technology
Hellenic Open University
Patras, GR-26335, Greece

[2]Archirodon Construction (Overseas) Co. Ltd
Block No.2, Green Community
Dubai, UAE

[3]Department of Civil Engineering, School of Engineering
University of Birmingham
Edgbaston, Birmingham, B15 2TT, United Kingdom

Abstract: Undertaken with industry, this paper analyses concrete-filled steel tube (CFTs) pile members in deep foundation systems under cyclic and seismic loads considering inelasticity for both pile and soil. Real seismic events have pointed out that piles may fail by forming multiple plastic hinges at various location or global buckling instability. This study confirms that CFT piles efficiently reduce damage in pile-heads and over the pile length, in depths that is difficult to access and repair the damage. The paper performs a set of analyses that enables understanding of the nonlinear mechanical behaviour of CFT piles and soil-structure interaction effects. The capacity margins of the novel foundation system are firstly assessed through controlled loading analyses (i.e., monotonic and cyclic loading histories), and then investigated further by a two-level seismic-intensity analysis. CFT pile damage patterns, displacement profiles and residual displacement are discussed and compared with those of corresponding concrete piles. Moreover, comparisons with four test campaigns taken from the literature confirm the correctness of the adopted nonlinear models for soil-pile interaction and soil inelasticity. Although its simplicity, the developed p-y modeling can successfully account for soil degradation effects making possible the simulation of the rather demanding, but advanced "s" shape of soil's cyclic behaviour, allowing for a reasonable comparison between composite and concrete piles. While the damage areas of both CFT and RC piles are mainly developed in pile heads and stiffness-discontinuous soil layers, CFT piles exhibit a lower damage than that of the RC piles nearly by 40% on average.

Keywords: Soil-pile foundation; concrete-filled steel tubes; soil inelasticity; cyclic deterioration; seismic intensities; damage index.

1. INTRODUCTION

Pile foundations are used widely for supporting buildings, bridges and other critical infrastructures, i.e. wind turbine towers, oil and gas platforms, tanks, earth retaining walls, wharfs and jetties, aiming at safely transferring the structural loads to the ground without excessive settlement and/or lateral movement of the structure. However, recent research has demonstrated that axial load alone can cause a slender pile to fail by forming plastic hinges due to local buckling related failures or global buckling instability [1]. Studies have shown that piles founded in soft clay can fail by buckling, as well as they can fail by shear, bending or axial loads during earthquakes [2]. One major effect is the arise of significant strains in weak soils that induce bending moments on piles in presence of a high stiffness contrast in a soil deposit [3]. Seismic events like the 1964 Niigata earthquakes and the 1995 Kobe earthquake have also reported pile failures in liquefiable soils during earthquakes in buildings, bridges and LPG tanks [4-6]. New foundation systems with controlled inelastic behaviour are under development to provide satisfaction of the improved design methods to multiple failure criteria [7, 8].

The last two decades, the use of concrete-filled steel tubular (CFT) columns has been continuously increasing especially in heavy constructions and critical infrastructures, such as high-rise buildings, bridges, towers [9, 10]. Compared with the traditional reinforced concrete or steel only columns, CFTs exhibit many advantages. They offer a large strength per cross-section area ratio combined with high ductility and energy abortion capacity. At high inelastic levels the concrete infill constrains inward local buckling of the steel tube, thus limiting the deterioration of strength and stiffness [11-14]. As a result, the increased ductility of CFT columns reduces the strength demands in structures at the preliminary stage of their design resulting in more compact and economical cross-sections [15]. Over the last years, various studies [16-23] have investigated the flexural behaviour of rectangular and circular CFT columns under different levels of constant axial loads. Advantages of circular CFT columns over other types of CFTs (i.e., square and rectangular), such as greater moment enhancement ratios due to the larger level of confinement of the concrete core, higher flexural strength and ductility has also been highlighted. Similar findings have been seen in [24, 25] where circular CFT columns presented mainly hardening and rarely softening behavior. Recent experimental studies [17, 26] on circular CFT columns made of high and ultra-high strength steel suggested a further delay of local buckling indicating that an even larger strength per column weight can be achieved.

The use of CFTs, therefore, as piles in foundation systems can potentially lead to damage reduction either in local or global level adding resilience in critical infrastructures, particularly for deep foundations that are difficult to access, monitor and repair in the events of strong loading events. At the same time, by combining a CFT column with a CFT pile appears to be attractive in terms of construction efficiency as the same member used in superstructure is embedded within the soil, thus enhancing the construction efficiency of the system. The presence of steel tube serves as both the reinforcement and formwork for concrete core until deep soil levels ensuring that the tube and the inner core can effectively transfer the target load. Such a pile foundation system can combine both the advantage of steel piles (high bending and shear strength) and concrete piles (large compressive strength and lateral stiffness). This effective combination enhances lateral stiffness and strength and can successfully address a possible discontinuity of the lateral support due to soil failure (e.g., softening, liquefaction) [27] as well as delay the formation of plastic hinges. CFT piles have not yet gained the worldwide acceptance compared to the traditional piling systems [28] as it is a new structural system, and no systematic investigation on their inelastic behaviour has been carried out yet, but a few recent studies [29-31] have shown that they can be efficiently used in deep foundations. Recently, Li et al [32] conducted tests in double-CFT-pile foundations under cyclic loads. The soil around the piles was neglected in their study as emphasis was given to simulate the elevated pile foundations or the pile foundations subjected to scour. The present study aims to investigate the inelastic response of CFT soil-pile foundation systems under both monotonic, cyclic lateral and earthquake loads having a specific target to evaluate the performance of CFT piles in terms of local and global damage considering soil-pile interaction effects.

Generally, for understanding the behaviour of pile foundations as a system and support the development of simulation methods, earlier works conducted laboratory or field experiments involving general pile groups under monotonic and cyclic lateral loading [33-35] to elucidate the ultimate state of these deep foundations during strong earthquakes. Several numerical methods have been developed and used by many researchers to consider many types of soil and deep foundation geometries compared to field and laboratory tests [36, 37]. Numerical approaches are recently performed using three-dimensional (3-D) elastoplastic finite element methods (FEM) based on realistic pile models and soil behaviour [37-40], while during the last decades, FEMs were used to examine coupled semi-infinite soil-pile foundation systems [41, 42]. Although, the entire coupled system can be analyzed simultaneously in FEMs, simplified modeling approaches are still attractive alternatives due to their low computational cost.

Simplified pile simulation approaches utilize distributed boundary springs along the length of the pile to simulate the soil-pile interaction force as nonlinear function of the pile displacement at given depth. The nonlinear Winkler foundation method (or p-y model) is considered as an attractive method, because of its simplicity and reliability [43-46]. Moreover, the p-y model is effective in accounting for the layered soil profile, nonlinear interaction and the depth-varying ground motions and has been applied in many cases to simulate the whole soil-foundation system [47, 48]. To obtain the bending moment in a pile affected by inertial or kinematic loading as well as analyze the behavior of a structure supported on a pile embedded in a layered soil, the accuracy of estimation of the pile-soil stiffness has crucial role for cyclic nonlinear soil–pile interaction effects [43]. Nevertheless, a discussion between simplified design approaches and efficient numerical/computational models [44, 49] for the realistic simulation of the cyclic and dynamic behaviour of soil-pile foundations does exist. The present study balances acceptable accuracy with the computational efficiency by considering the soil-pile interaction effects and soil inelasticity incorporating the static p-y curve approach with strength and stiffness degradation effects within the frame of a Winkler model. At this first stage of investigation of the inelastic mechanical behaviour of CFT piles, a simple, yet efficient, analytical/numerical method for soil-pile interaction is considered.

This study investigates the inelastic behavior of a real-word project founded in a 40m-thick soil stratigraphy characterized by in-situ measurements. The model for the foundation system is developed with the aid of RUAUMOKO analysis program [50] under plain strain conditions using hysteretic behaviour models. Initially, the inelastic behaviour of soil is investigated under monotonic lateral and cyclic loading, and suitable mechanical values (i.e. bilinear factor, yield pressure, initial stiffness etc.) are determined via useful forms of equations which have been developed in [43] within the frame of a Winkler model. All of these are incorporated in a typical p-y model in order to simulate the nonlinear soil-pile interaction in an accurate enough for the purpose of this study way. Although its simplicity, current p-y modeling accounts for soil degradation effects making possible the simulation of the rather demanding “s” shape of soil’s cyclic behaviour for the advanced stiffness degradation state. The proposed analytical/numerical model is compared with existing computational and experimental results and its accuracy and efficiency is demonstrated. Then, the soil-pile foundation system is subjected to various lateral monotonic and cyclic loading histories up to high inelastic levels, as well as to two sets of seven ground motions compatible with two levels of seismic intensity: the design basis earthquake (i.e., 10 percent probability of exceedance in 50 years) and the maximum occurring earthquake (i.e., 2 percent probability of exceedance in 50 years). The inelastic behaviour of the pile foundation is evaluated in terms of damage patterns and displacement profiles of the piles, energy dissipation capacity and residual displacements of the system. For completeness, the results are compared with those of a corresponding reinforced concrete (RC) structure that utilizes concrete piles embedded into the same soil stratigraphy. The inelastic behaviour of the RC member including pinching and strength deterioration is considered and verified with experimental findings. The results of this investigation reveal that CFT piles perform better than RC ones, significantly reducing damage and inelastic displacements of the structure as well as in some cases the very critical residual displacements. This difference arises from the beneficial inelastic behaviour of CFT members, such as, high resistance to buckling related failures and hardened post-peak flexural strength. The soil inelasticity revealed to be beneficial in absorbing an amount of input energy and relieving the damage of piles, particularly in upper more soft layers of the soil stratigraphy.

The paper is organized as follows: Section 2 and 3 describe the proposed composite soil-pile foundation system and the solution of p-y model used for the simulation of the inelastic behaviour of the soil, respectively. Section 4 describes the hysteretic models used for the simulation of the inelastic behaviour of the CFT and RC piles as well as it presents validation results for the inelastic simulation of the soil-structure system. Section 5 compares the behaviour of CFT and RC pile foundation systems under monotonic lateral and cyclic loads in terms of damage patterns, damage index profiles and displacement profiles at various inelastic levels. In a similar manner with Section 5, Section 6 analyzes the seismic behaviour of the pile foundation systems under two sets of seven ordinary ground motions scaled on the corresponding intensity levels. In addition to maximum and mean damage indices, the hysteretic behaviour and displacement histories of critical ground motions are presented and discussed. The paper closes with the conclusions of Section 7.

2. STATEMENT OF THE PROBLEM STUDIED

A composite soil-pile foundation system is modeled under conditions of plane strain considering soil inelasticity. The system consists of a group of three circular CFT piles inter-connected through a rigid deck (pile cap) on their heads to distribute the forces equally to the piles of the group. The CFT piles are embedded into an inclined layered soil, fixed at the bedrock, which supports the layered soil as shown in Fig. 1(a). The free heights of the three piles from the free soil surface to the pile-head are 4.0, 8.0 and 12.0 m from the left to the right, respectively, defining different moment-to-shear ratios for the free length of piles. This model was developed on the basis of a real-world project located in the Arabian Gulf [51]. The project includes marine works for the extension and strengthening of a port. The behaviour of the proposed structure/foundation system is investigated under monotonic lateral and cyclic lateral as well as under seismic loads of two levels of seismic intensity. As shown in Fig. 1(a), the lateral action is applied to point A, which has a distance 0.50 m from the head of the left pile, in the form of lateral force or lateral displacement for the case of monotonic and cyclic loading, respectively, to have a better control of the displacement history through the rigid cap. For the seismic, analysis the inertia forces are imposed from the vibration in the whole structural mass and control through point A is not necessary.

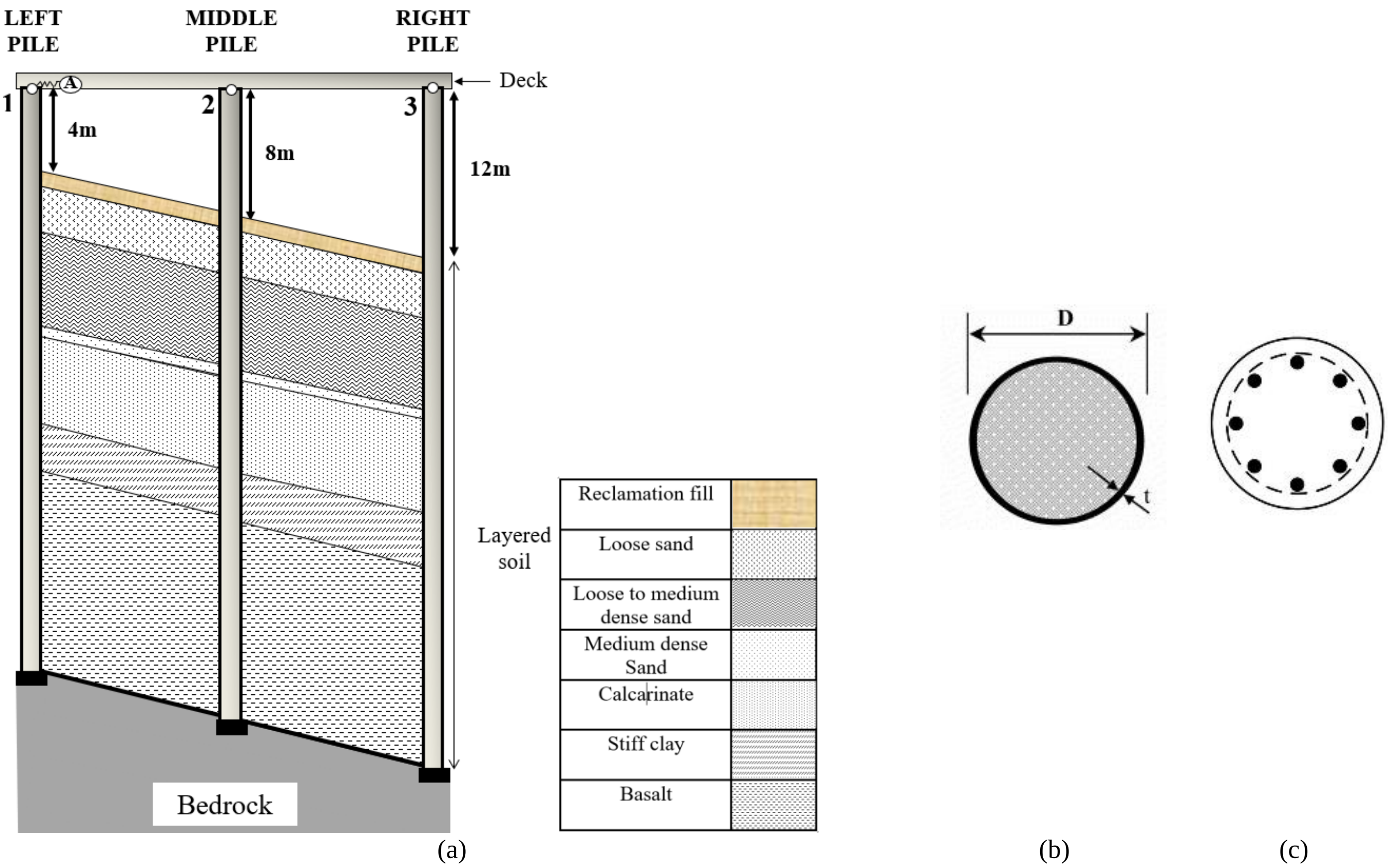

Figure 1: (a) A typical examined soil-pile foundation system consisting of circular piles and seven different soil layers with inclination; (b) circular CFT cross-section and (c) circular RC cross-section

2.1 Characteristics of soil layers

A boring log shows a layer of silt / sand of 35 meters below seabed level overlying a layer of completely to moderately weathered basalt to tip of the pile. SPT N Values for the soft materials vary from 7 to 33. The pile is to be driven through a 40m-thick relatively soft ground (loose to medium dense silty sand to sandy silt), underlain by the bedrock, as shown in Fig. 1(a), which has gradually increasing strength in the upper 5m (weathered zone). The soil also exhibits a gradually increasing strength in the upper 5 m (weathered zone). Table 1 shows the complete soil stratigraphy of the region under consideration. According to the p-y modeling [43] soil is assumed to be bilinear elastoplastic and its interaction with the piles is modeled by non-linear horizontal springs of the Winkler type. During cyclic and seismic loading, soil strength and stiffness degradation is considered as discussed in a later section. The horizontal springs along the pile’s height have placed every 1 m. In general, the soil stratigraphy effect requires the determination of six-physical parameters for each type of soil, such as the Young’s modulus, the internal friction angle, the effective unit weight, the horizontal earth pressure, the shear strength and the initial stiffness. It is worth noticing, that current soil stratigraphy is based on in-situ measurements. Table 1 presents a few more parameters for the soil layers while the complete set of information can be found elsewhere [51].

Table 1: Characteristics and parameters of soil stratigraphy

Depth (from layered soil)	Soil classes	Angle of internal friction φ (degrees)	Initial stiffness k (kPa/m)	Shear strength c_u (kPa)
+1.13m to -0.87m	Reclamation fill	-	16,287	-
-0.87m to -6.87m	Loose sand	30	5,4290	-
-6.87m to -14.87m	Loose to medium dense sand	32	10,858	-
-14.87m to -15.87m	Medium dense sand	35	16,287	-
-15.87m to -27.87m	Weak calcarenite rock	45	33,931	-
-27.87m to -33.87m	Stiff clay	-	-	100
-33.87m to -41.87m	Basalt rock	-	-	400

2.2 Characteristics of CFT and RC piles

For comparison, a corresponding reinforced concrete (RC) infrastructure that utilizes concrete piles embedded into the same soil stratigraphy with the CFT system is also investigated. Figure 1b shows the cross-sections of the piles considered. All three piles of the examined structure have the same dimension characteristics and material properties. More specifically, the diameter (D) of the CFT piles is equal to 1067 mm, the steel tube thickness (t) of the steel tube is equal to 19 mm, while the tensile yield strength (f_y) and the compressive strength (f_c) are equal to 485 and 30, respectively, expressed in MPa. The viscous damping ratios for CFT piles and RC piles are equal to 0.03 [52] and 0.05 [53] respectively. Regarding the RC piles, the total number of the reinforcement steels was found to be 78ø32 based on Eurocode-2 [54] achieving approximately the same yield flexural strength with the CFT piles. Finally, the weight applied to each pile-heads is equal to 10,200 kN which defines an axial strength ratio around 0.2-0.23.

3. SOLUTION OF THE PROBLEM

3.1 P-y soil-pile modeling interaction

The popular subgrade reaction model, typically known as Winkler model, is widely used for the determination of the behaviour of the soil-pile foundation system under static lateral loading because of its simplicity and efficiency, as illustrated in Fig. 2(a). The main parameters of a load-displacement (p-y curve) relationship are stiffness and strength. The stiffness of p-y curve is the resistance of soil to unit pile deformation. During transient vibration, the stiffness of soil plays an important role. Figure 2(b) depicts the behavior of the soil-pile foundation system when its movement is either small or large. For analysis of a pile subjected to lateral loads, the soil surrounding the embedded length of the pile is idealized as distributed Winkler-type springs which resist lateral displacements of the pile. For modelling purposes, the pile is laterally supported by bi-linear elasto-plastic springs with degradation effects was can be seen in a later section. In this study, springs were placed every 1 m.

In general, p-y curves are highly nor linear, and can be either monotonic or have a softening/degradation part. Initially, at small horizontal displacements, the soil response is linear. The response becomes progressively non-linear as the displacements increase. Ultimately, the soil response assumes a constant value p_{ult}, that does not increase with further increase of the horizontal pile displacements. The ultimate pressure corresponds to failure of the soil around the pile either in the form of passive failure of a soil wedge or of soil flow around the pile. The shape of the p-y curves is highly dependent on the soil properties and the loading characteristics.

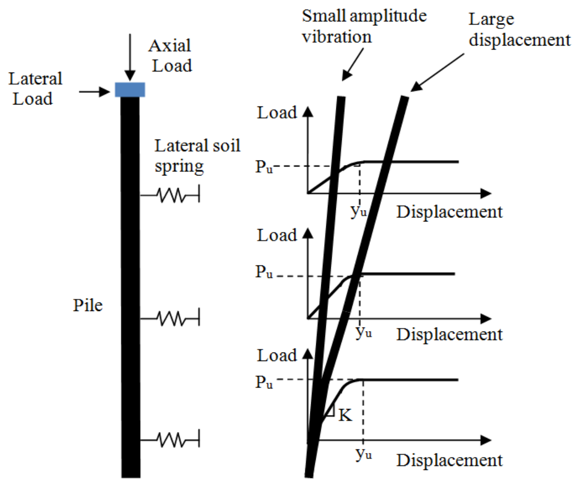

(a) (b)

Figure 2: (a) Modeling of a typical pile element, (b) soil-pile interaction for small and large amplitudes of soil-pile lateral movement

3.2 Solution procedure

The horizontal springs for every soil layered are placed around each CFT and RC pile. Their yield force F_y and stiffness K, expressed in kN and kN/m respectively, are connected through the relation

$$F_y = K \cdot u_y \tag{1}$$

where u_y is the yield displacement of the spring in m. The expressions

$$K = k_{sh} \cdot D \cdot t \tag{2}$$

and

$$u_y = \frac{P_{ult}}{k_{sh}} \tag{3}$$

where k_{sh} is the equivalent stiffness expressed in kPa/m. D is the pile diameter and t the distance between the springs as layer thickness expressed in m. In this study, t is equal to 1.0 m. The k_{sh} for sand soils (i.e. reclamation fill, loose sand, loose to medium dense sand, medium dense sand and calcarenite) is given by

$$k_{sh} = \alpha \cdot k \cdot z \tag{4}$$

where z is the depth in m and k is the initial soil stiffness in kPa/m taken from Table 1. Using the least-squares method for minimizing the error, the non-linear p-y curve is approximated by a bi-linear expression. The approximation factor α was found to be 0.769. In Eq. (3), P_{ult} is the ultimate load in kN and can be computed for sand soil layers as

$$P_{ult} = p_u \cdot n \cdot A \tag{5}$$

where p_u is the soil resistance expressed in kN, n is the geometry factor taken equal to 1.0 for prismatic piles and equal to 1.5 for tapered piles. In this study, the geometry factor n is taken as 1.0. In addition, $A = 3 - 0.8(z/D) \geq$

0.9 for static loads or equal to 0.90 for cyclic loads. Further information about the computation of the soil resistance, p_u, as well as the above procedure for stiff clay and basalt rock under monotonic and cyclic loads can be found in [43, 51].

4. PILE MODELLING AND VALIDATION OF THE SOIL-PILE FOUNDATION SYSTEM

4.1 CFT and RC piles

The inelastic behaviour of the examined structure models are investigated with the aid of Ruaumoko analysis program [50]. As shown in Fig. 3(a), the RC piles are modeled using the well-known Clough hysteretic model [50] (same as the modified Takeda hysteretic model [50] which is part of Ruaumoko analysis program [50]). Based on this model the bilinear factor r is equal to 0.02 whereas the strength degradation of RC piles can be approximately 20% or more, according to Park/Kent model [55]. In this study, the cyclic strength reduction is assumed to be 30% of the corresponding ultimate monotonic strength [56]. In Ruaumoko, the strength reduction variation is introduced through the ductility, as shown in Fig. 3(b). Three parameters are defined: DUCT1 ($=d/d_y$), which is the ductility at which the strength degradation begins; DUCT2, which is the ductility at the end of strength degradation; and RDUCT, which is the residual strength as a fraction of the initial yield strength. DUCT1 and DUCT2 was taken equal to 2.0 and 10.0, respectively [53]. Degradation parameters were adopted only for the cyclic and seismic analyses.

The inelastic cyclic behavior of circular CFT piles is simulated using the Ramberg-Osgood hysteretic model [50] (Fig. 3(c)) as proposed in [12]. In Fig. 3(c), the first equation is valid for the initial loading (path 1-2) or monotonic loading, while the second equation is valid for unloading and reloading (path 2-3-4). The transition between the elastic and plastic branch, is controlled by the Ramberg-Osgood factor r_2 whose influence is shown in Fig. 3(d). The factor r_2 is computed by employing the associated expression in [12] and is different for the monotonic and cyclic response in order to account for cyclic hardening and the increasing confinement levels. Strength degradation is limited in circular CFT members as has been seen in experimental researches [17, 57, 58], thus only a strength degradation of 5% is considered in this study at the inelastic level of 20. The horizontal spring parameters are determined by employing Eq. (1) for each soil type introduced above. Regarding soil, a constitutive model under cyclic shear loading must be able to characterize the behaviour both at small and large strains and consider the effects of strength and stiffness degradation phenomena and the load history at the soil response [49]. A stiffness-degrading bilinear model is sufficiently developed here to have taken the “s” shape in large strains and is obtained through the hysteretic behaviour model shown in Fig. 3(e). The cyclic shear strength reduction is accounted directly through the reduction factors of p-y model introduced in previous section.

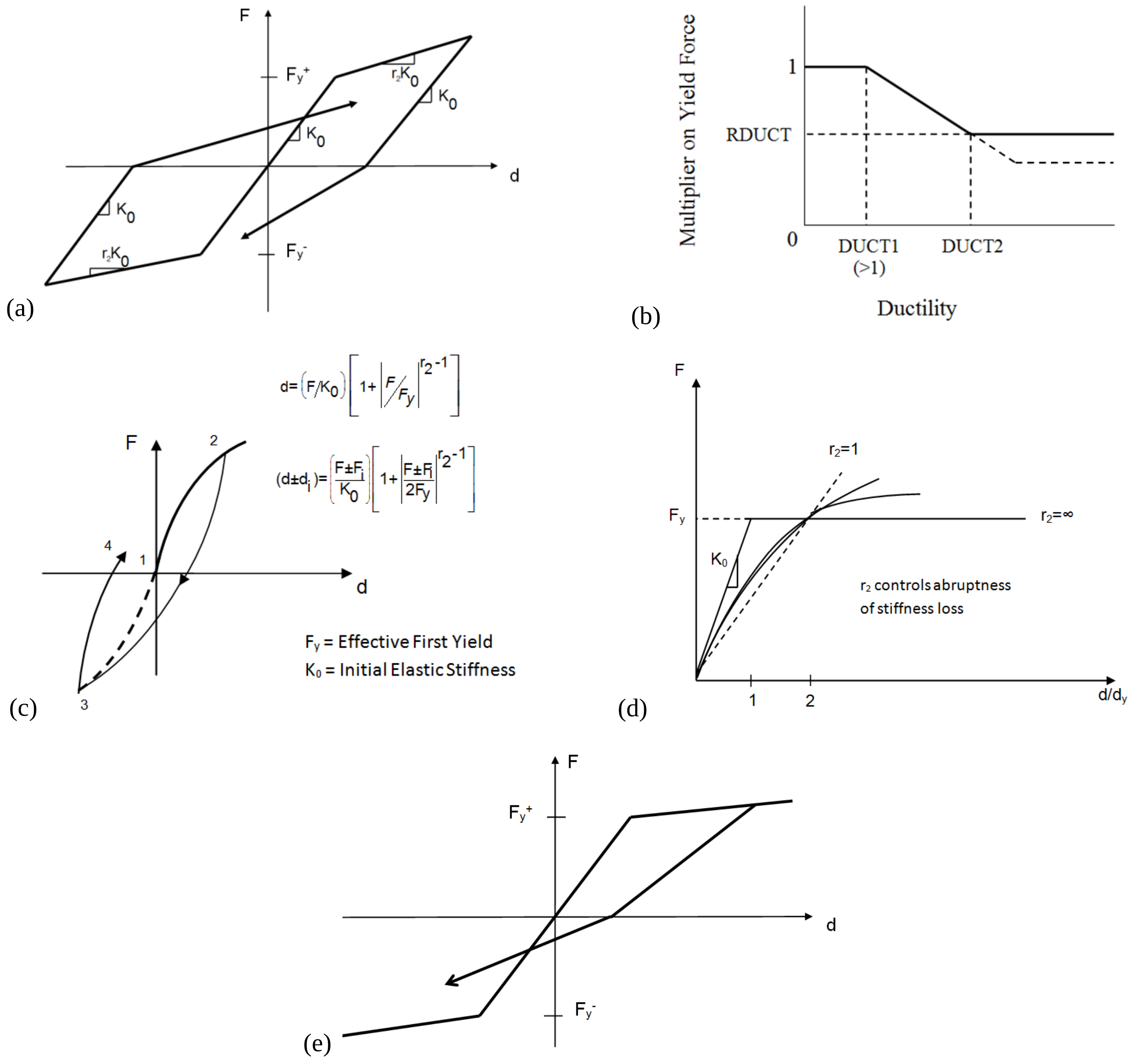

Figure 3: (a) Concrete hysteretic model; (b) in-cycle strength reduction variation using ductility terms; (c) CFT hysteretic model; (d) factor r_2; and (e) soil hysteretic model

4.2 Validation of the proposed analytical method

The reliability of the proposed approach is confirmed by comparing its results with computational and experimental results from the literature. The adopted computational data and results [59] are shown in Table 2 and Fig. 4(a), respectively. The results are related to the lateral behaviour of a single pile embedded into sand consisting of circular RC cross-section. Experimental data and results used here for comparison [60], are shown in Table 3 and Fig. 4(b), respectively. The results are related to the lateral behaviour of a pipe RC cross-section embedded into a soft clay. In addition to this, one more experiment was adopted from the literature [35] for comparison. In this test, the monotonic and cyclic behaviour of a single pile embedded into sand and clay consisting of hollow circular RC cross-section was examined. Table 4 provides the test parameters, while Fig. 5 presents the comparisons between the proposed model and test results.

On the basis of Fig. 4 and Fig. 5, one can see that the proposed analytical method can describe with reliable way the monotonic and cyclic lateral loading responses of concrete piles including various geometrical and material properties both for the piles and the soil. The stiffness and strength have been traced with fairly good accuracy for both case studies. An example of particular importance is the comparison for the second test shown in Fig. 5 where both the monotonic (Fig. 5(a)) and cyclic (Fig. 5(b)) test refer to the same pile [35]. Compared with the monotonic loading, the lateral load-carrying capacity of the pile under reversed cyclic loading had degraded by 28%. This amount of strength degradation was sufficiently captured by the proposed model. The degradation in lateral load-carrying capacity in reversed cyclic loading is due to the combined degradation in concrete modulus and soil shear modulus with cyclic loading. Therefore, although its simplicity, current p-y modeling accounts for soil degradation effects making possible the simulation of the "s" shape of soil's cyclic behaviour for the advanced stiffness degradation state.

Finally, flexural failure was observed in both monotonic and cyclic tests of Ref. [35] due to failure of the longitudinal reinforcement. The maximum damage locations for the monotonic specimen and cyclic specimen were found to be at a depth of 0.6 and 1.2m from the ground level (GL), respectively, as shown in Fig. 5(c). It can be seen in this figure, that a quite similar damage pattern was identified by the proposed analytical method. The gradual progress of the cyclic damage in deeper levels than in monotonic damage is likely to be related to the reversed cyclic loading and degradation effects.

Table 2: Pile and soil parameters of computational results in [59]

Pile parameters	Length L(m)	Outer diameter D (m)	Yield stress f_y (MPa)	Compressive strength f_c (MPa)	Number of reinforcement steels	
	14.25	0.508	413.69	34.47	12ø8	
Soil parameters	Total united weight γ (kips/in^3)	Shear modulus of vertical soil G (MPa)	Internal friction φ (degrees)	Soil modulus k (MPa)	Poisson's ratio v	Pile-soil face τ (MPa)
	5.60E-5	20.88	39	0.621	0.3	0.0696

Table 3: Pile parameters of test experiment in [60]

Pile parameters	Length L(m)	Outer diameter D (m)	Moment of Inertia I_p (m^4)	Poisson's ratio v	Yield bending moment M_y (kNm)
	12.8	0.319	1.44x10^{-4}	0.3	231
Soil parameters	Total united weight γ (kips/in^3)	Back-calculated undrained shear strength C_{uc} (kPa)		Poisson's ratio v	Elastic modulus Es (kPa)
	20	23		0.495	1600

Table 4: Pile parameters of test experiment in [35]

Pile parameters	Length L(m)	Outer diameter D (m)	Thickness t (m)	Compressive Strength of concrete f_c (MPa)	Yield stress of longitudinal prestressing steel f_c (MPa)	Effective prestress on the concrete piles (MPa)	Yield bending moment M_y (kNm)	Ultimate bending moment M_u (kNm)
	26	0.30	0.60	69	1325	5	42	51.2
Soil parameters	Soil type	Depth from GL	Saturated unit weight (kN/m^3)		Shear strength (kPa)	Shear modulus (MPa)	Poison's ratio (v)	
	Clay	0-6 m	15.7		33	20.4	0.5	
	Sand	6- 12.5 m	18.6		140	154.3		

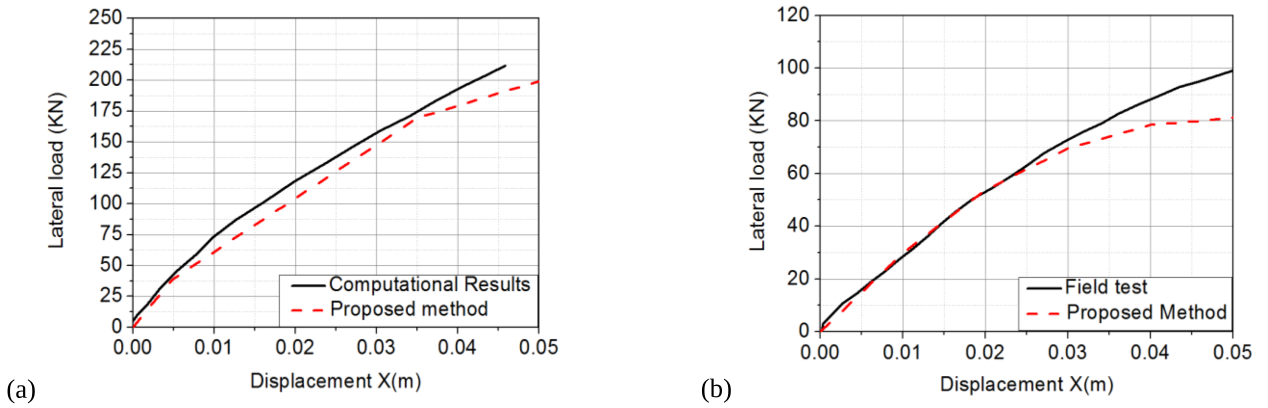

Figure 4: Comparison of the proposed method with results under monotonic lateral loads from the literature: (a) computational results [59]; (b) experimental results [60]

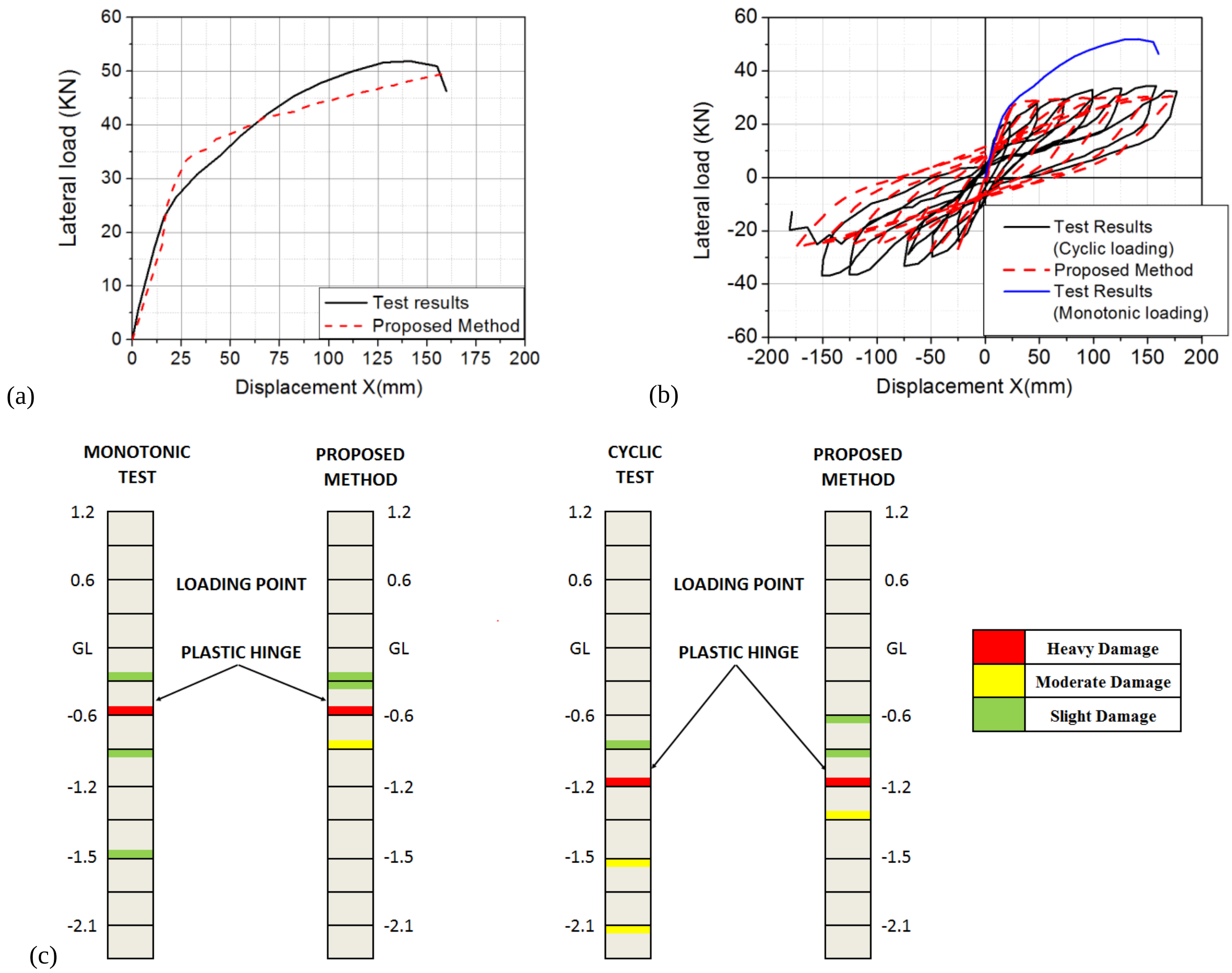

Figure 5: Comparison of the proposed method with results under monotonic lateral and cyclic loads from the literature [35]: (a) monotonic test; (b) cyclic test and simulations with pile and soil degradation; (c) damage pattern in pile (monotonic and cyclic test)

5. STATIC INELASTIC ANALYSES OF THE SOIL-PILE FOUNDATION SYSTEMS

5.1 Lateral behaviour under monotonic and cyclic loads

In this section, comparisons between CFT and RC soil-pile foundation models under monotonic and cyclic lateral loadings are presented. Figure 6(a) shows the monotonically increasing applied force for the cases where the soil layers flexibility is both considered and ignored for comparison. The applied force starts from a zero value and reaches maximum values nearly of 11,600 kN for rigid soil, and nearly of 6,200 kN when soil-pile interaction is considered. The maximum induced displacement ductility in the whole system is $6u_y$, where $u_y = 0.09$ m denoting the yield displacement of the entire soil-pile foundation system (global yield displacement). Figure 6(b) plots the normalized moment by the plastic moment of resistance, M_{pl}, with the displacement ductility. The M_{pl} is equal to 10,510 kNm for the CFT cross-section and 10,724 kNm for the RC cross-section. The soil flexibility reduces the lateral stiffness of the system by 4.5 times reducing the shear strength demands within the examined global ductility of $6u_y$. The yield displacement, u_y, of the individual piles are 0.06 m, 0.11 m and 0.17 m for the left, middle and right pile, respectively.

Figure 6(c) shows the lateral cyclic displacement history, which consist of the displacement peaks 0.05 m, 0.09 m, 0.27 m and 0.54 m with corresponding to $0.045u_y$, u_y, $3u_y$, and $6u_y$ with two cycles imposed at each displacement level. Both monotonic and cyclic lateral loadings are imposed through displacement control algorithms. Figure 7 presents the cyclic response of the CFT soil-pile foundation model for the three pile-heads shown in Fig. 1, while in a similar manner with Fig. 7, Fig. 8 presents the response of the three pile-heads in terms of normalized moment – displacement ductility relationship. It is noted that in these figures, the lateral displacement has been normalized by the corresponding u_y of each pile, separately.

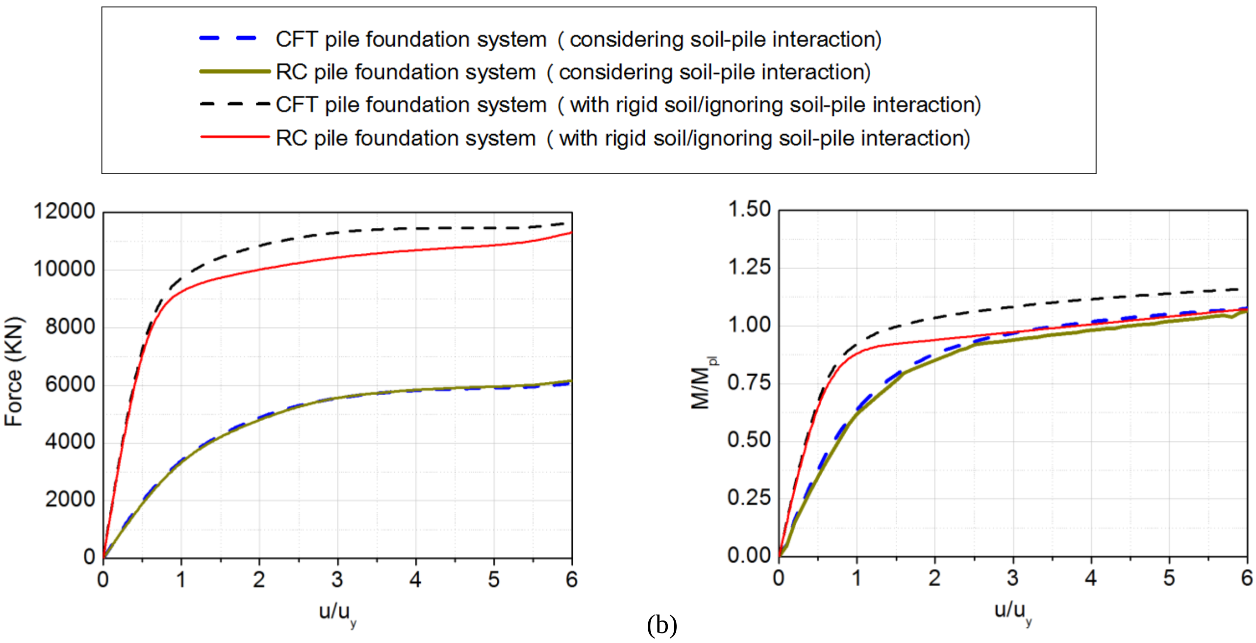

(a) (b)

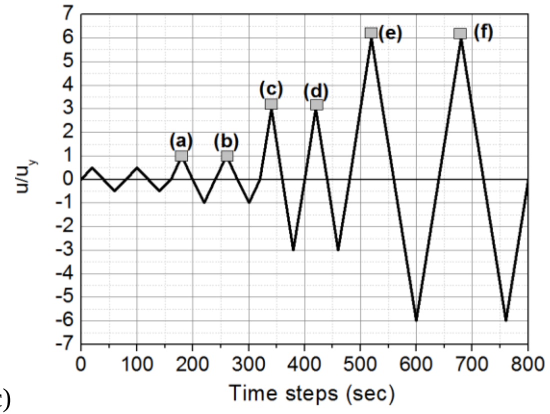

(c)

Figure 6: Monotonic lateral – displacement ductility relationship of the CFT and RC soil-pile foundation system considering and ignoring soil-pile interaction in terms of: (a) lateral force; and (b) normalized moment. (c) Cyclic lateral loading history for CFT and RC piles [62]

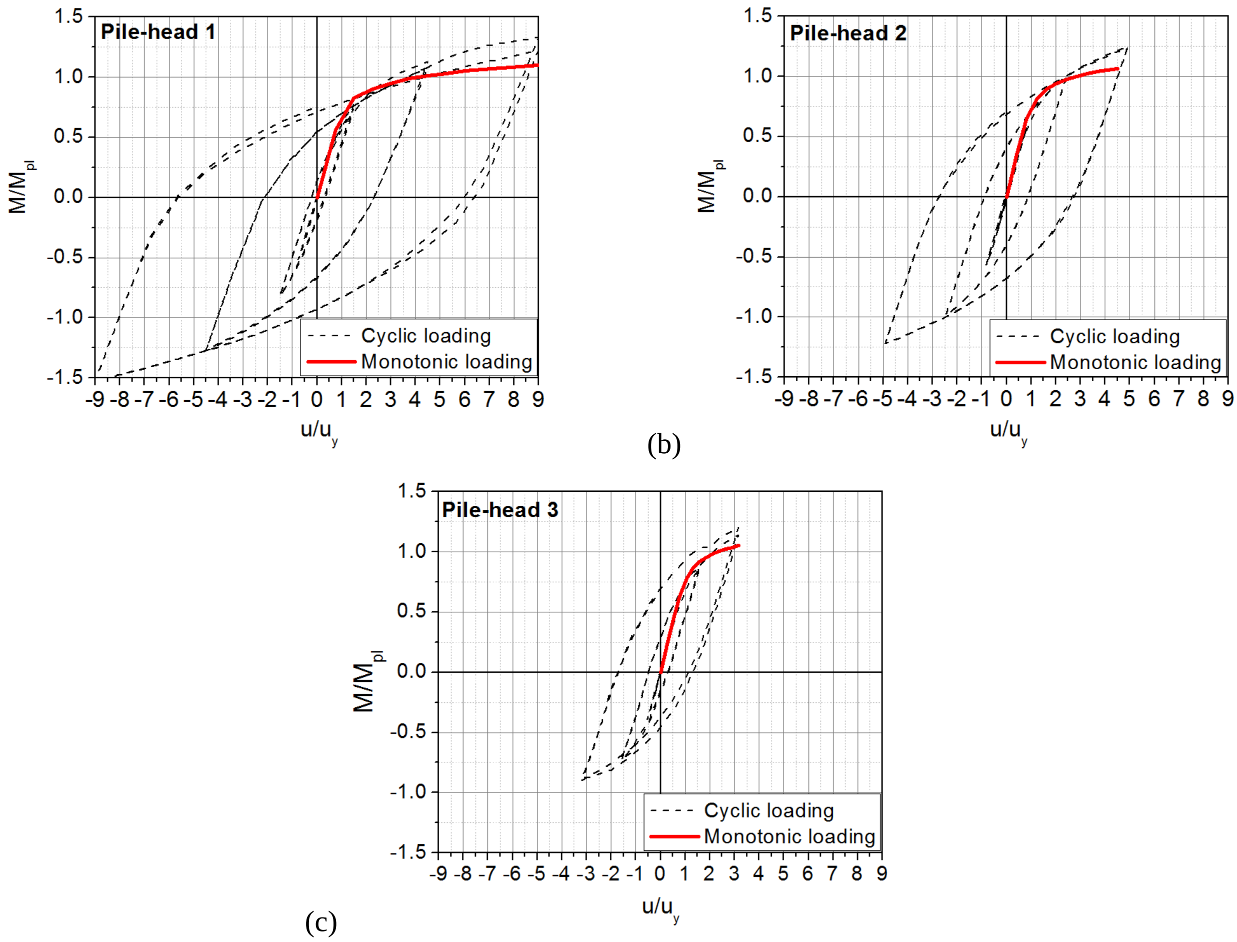

(a) (b) (c)

Figure 7: Monotonic versus cyclic lateral loading. Normalized moment – displacement ductility responses of CFT soil-pile foundation model for: (a) pile-head 1; (b) pile-head 2; and (c) pile-head 3

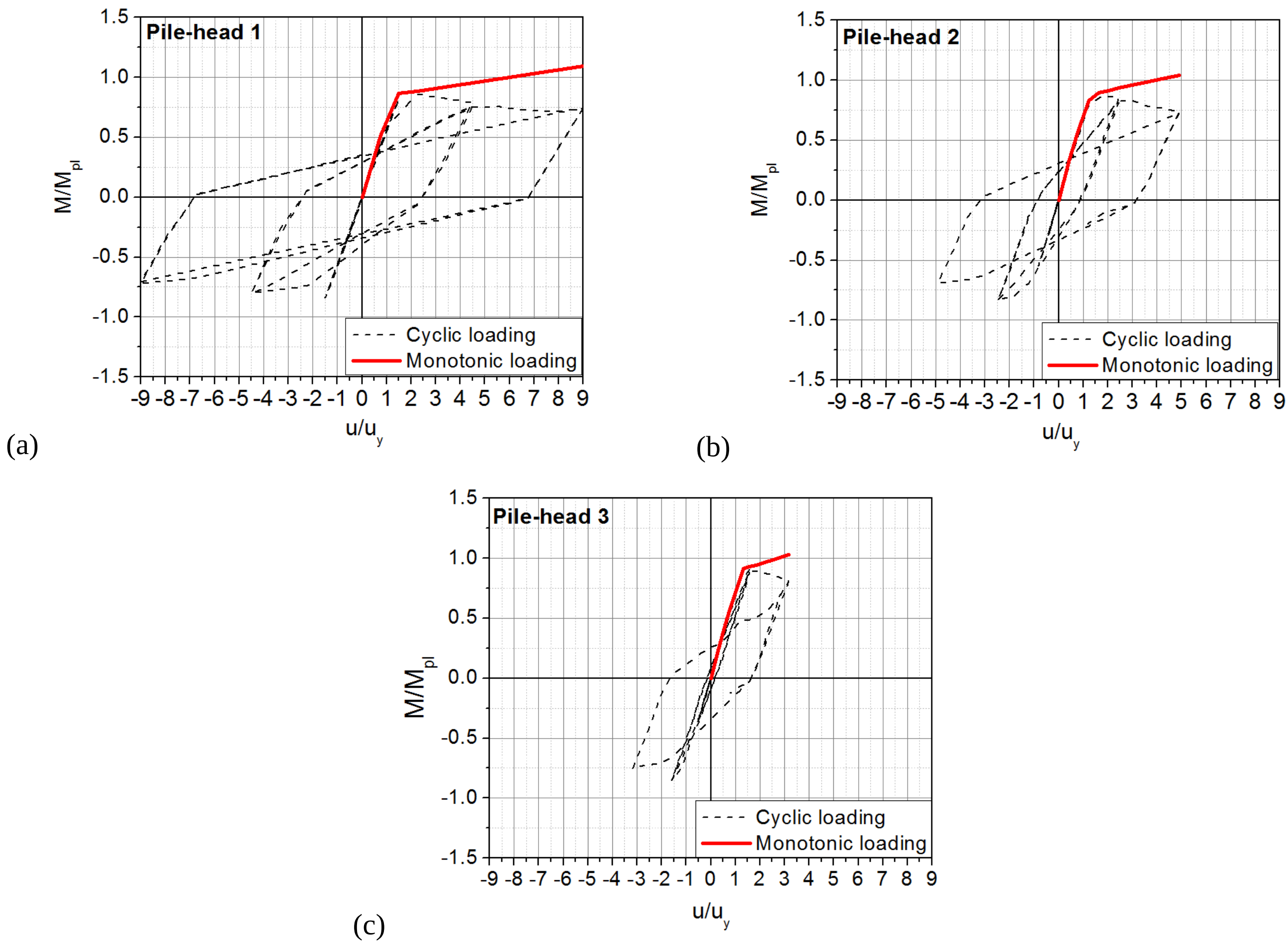

Figure 8: Monotonic versus cyclic lateral loading. Normalized moment –displacement ductility responses of RC soil-pile foundation model for the: (a) pile-head 1; (b) pile-head 2; and (c) pile-head 3

Figure 7 clearly validates the strong and fat hysteretic behaviour of CFT pile-heads. The response shows an appreciably high hardening and stable behaviour as well as in some cases a transient behaviour due to the cyclic hardening effect, i.e., in various loading phases the cyclic response is higher than the monotonic lateral response. This observation is in accordance with findings of [12] where similar results are shown for other member types. On the other hand, in the RC members shown in Fig. 8, the monotonic response is always higher than the peak values of the cyclic response due to strength degradation. The cyclic response of RC piles is characterized by a pinching and deteriorating behaviour which is expected to take place after cracking and yielding, particularly at large inelastic levels. During their cyclic response, a strength reduction nearly 25% of the original strength of the monotonic non-degraded response is observed. This is in accordance with the experimental findings in [35, 55, 56] and verifies the reliability of the developed model. For completeness, the responses of the examined soil-pile foundation models are compared under the same loads in Figs 9 and 10. Figure 9 compares the CFT and RC members under monotonic lateral loads, while Fig. 10 compares the same members under cyclic lateral loads.

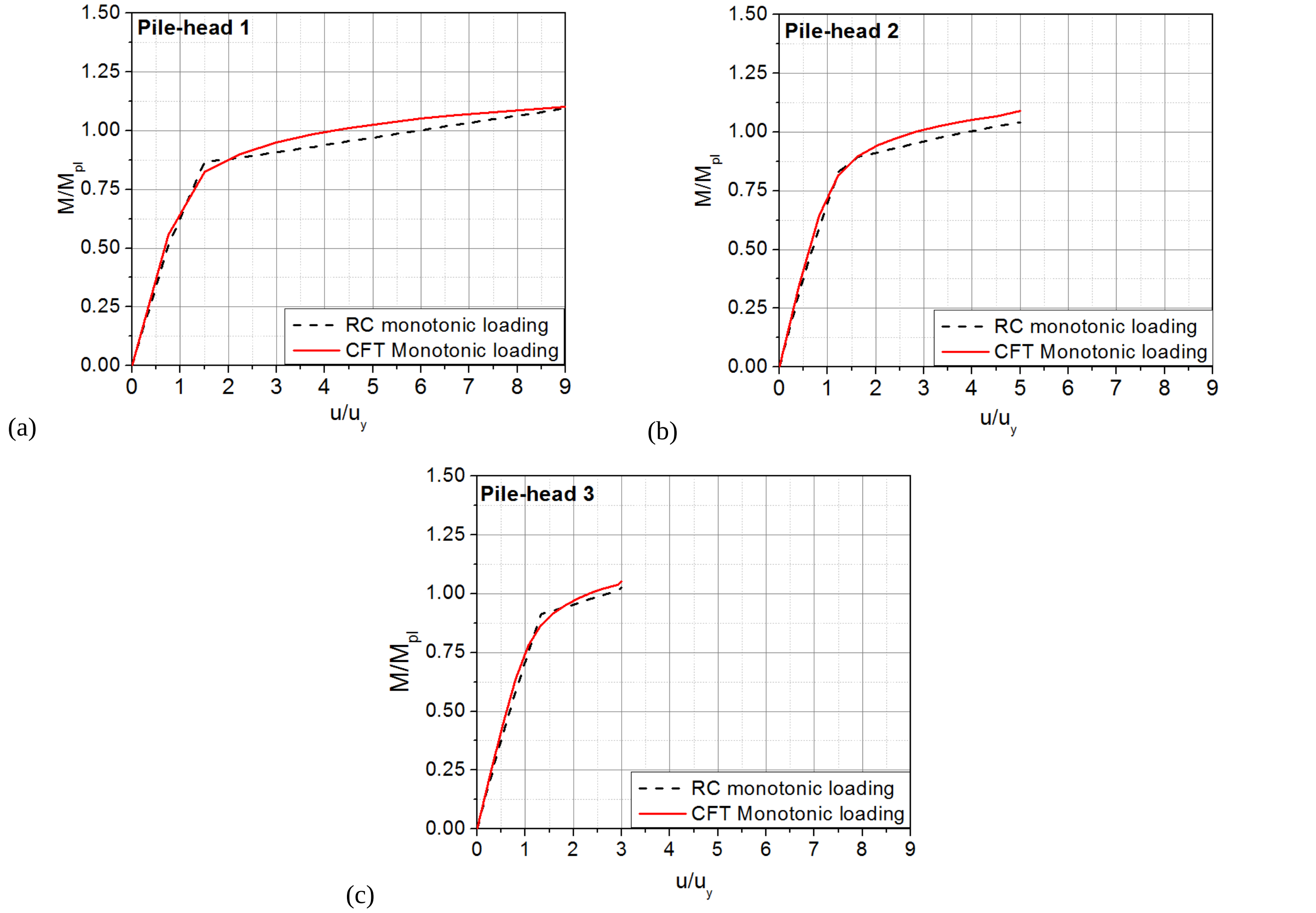

Figure 9: Comparison between CFT and RC soil-pile foundation models under monotonic lateral loading for the: (a) pile-head 1; (b) pile-head 2; and (c) pile-head 3

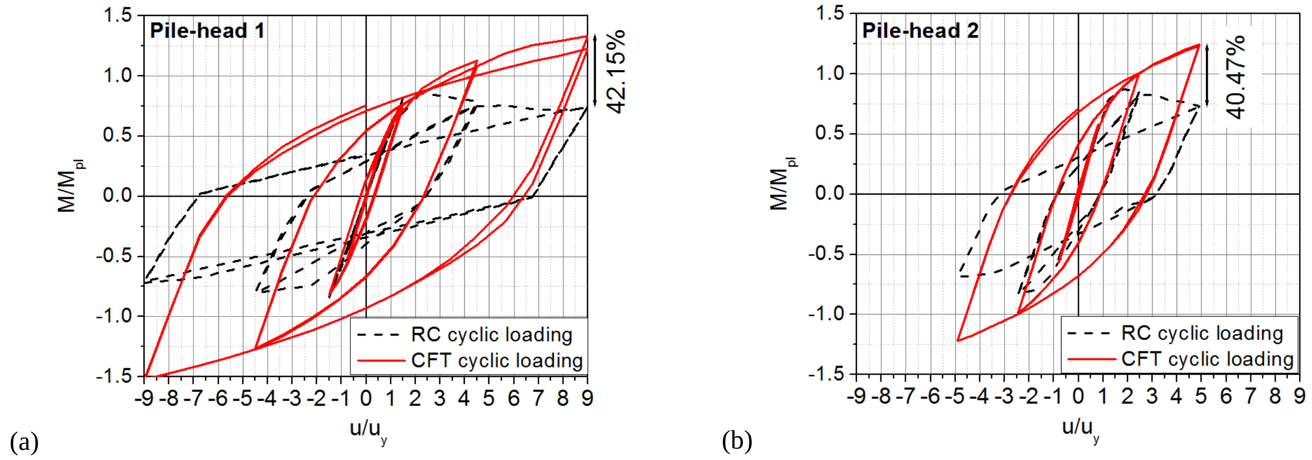

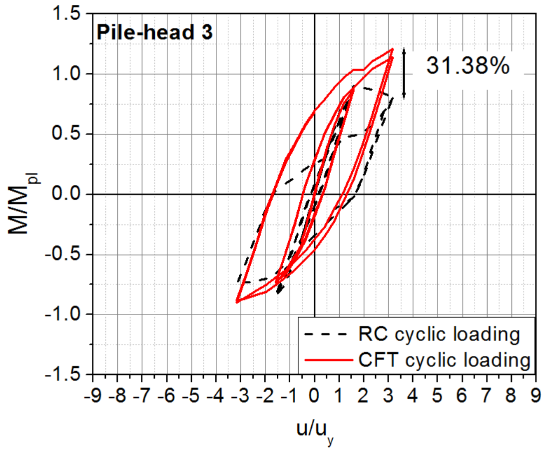

(c)

Figure 10: Comparison between CFT and RC soil-pile foundation models under cyclic lateral loading for the: (a) pile-head 1; (b) pile-head 2; and (c) pile-head 3

As shown in Fig. 9, both types of piles exhibit a similar initial stiffness and flexural strength confirming the design assumptions of this study. It is noted that strength degradation has been ignored for both CFT and RC piles under monotonic loads. A different behaviour is observed in Fig. 10 in terms of flexural strength. The maximum flexural strength of CFT pile-heads is 42%, 40% and 32% larger than the RC ones at a pile ductility level of 9.5u_y, 5.2u_y and 3.3u_y, respectively. In addition, the post-yielding strength of the CFT pile-heads tends to increase whereas the strength of the RC pile-heads has reached the maximum level at ductility level around 2u_y (plateau). The following section evaluates the energy dissipation capacity of the two piles through a damage index that accounts the amount of the absorbed hysteretic energy.

5.2 Damage and displacement analysis of CFT and RC piles

In this section, the damage index and the displacement profile of each CFT and RC pile along its height are investigated under the cyclic lateral loading. The Park-Ang damage index [62] is selected as the damage measure. The same index is adopted for the investigation of the seismic behaviour of the soil-pile foundation system as introduced at a later section. This damage index takes into consideration both the maximum deformation and the hysteretic energy of dissipation of structural members and is defined as

$$\mathrm{DI} = \frac{\mu_m}{\mu_u} + \frac{bE_h}{F_y \mu_u \delta_y} \tag{7}$$

where μ_m is the maximum ductility of the element, μ_u is its ultimate ductility and b represents a model constant parameter (usually, b=0.025-0.20) to control strength deterioration, E_h is the hysteretic energy absorbed by the element during the earthquake, F_y is the yield action of the element and δ_y is the yield displacement of the element. For reinforced concrete structures, the parameter b is equal to 0.05 [63]. In this research study, parameter b is set equal to 0.03 [52] for CFT members.

Figures 11-13 illustrate the damage and displacement analysis results. Figures 11 and 12 compares the damage patterns, regions and level of damage as occurred along the height of the CFT and RC piles for the cyclic loading at each global displacement ductility. Figure 11 gives more emphasis on the pile heads and in the region of the pile around the upper layers of the soil. Figure 12 presents in-detail the damage profile along the entire soil stratigraphy until deeper levels of soil. Accordingly, Fig. 13 compares the profile of the maximum displacements of the CFT and RC piles at each ductility level. In Figs. 12 and 13 depth is measured from the location of the pile cap.

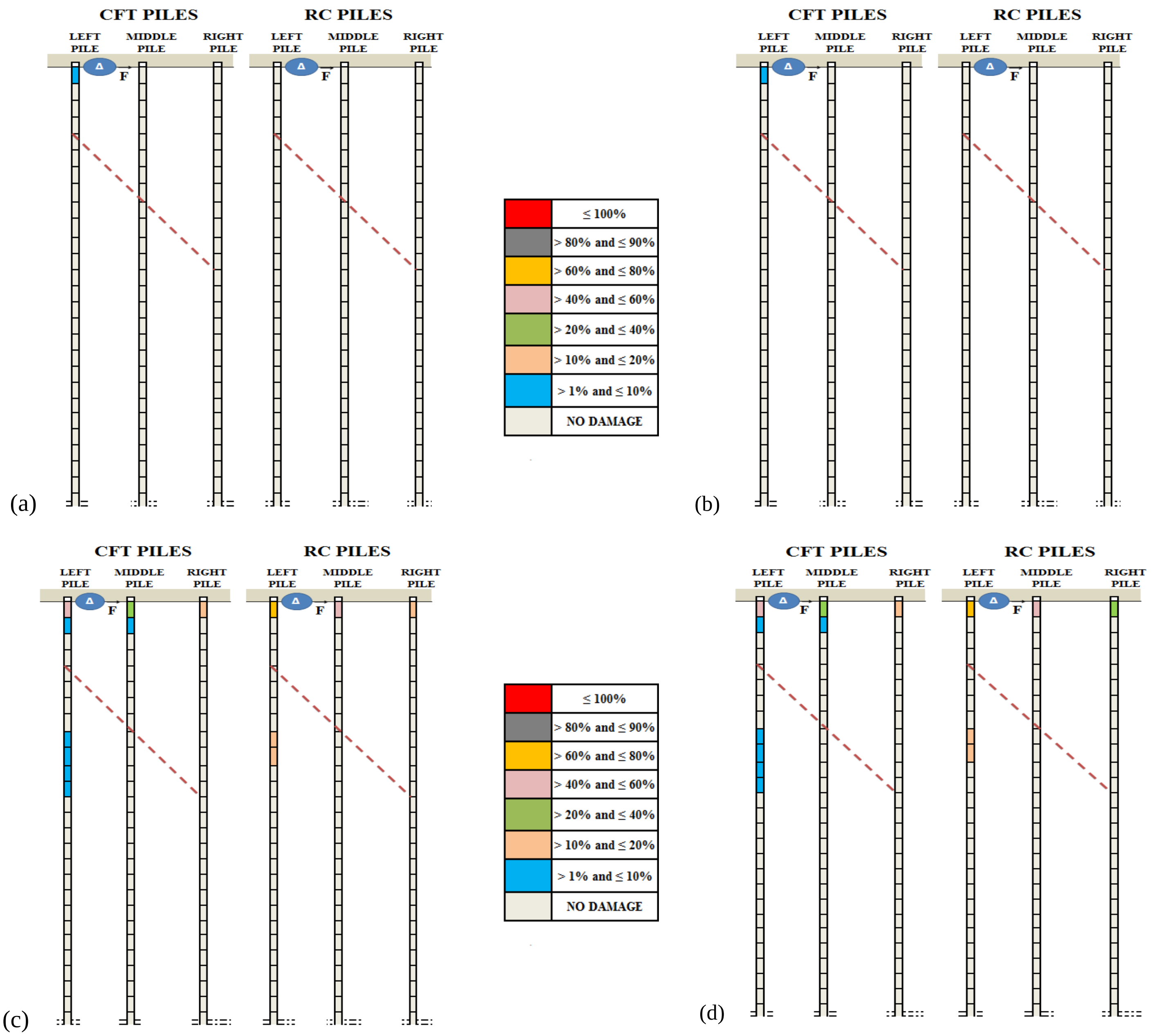

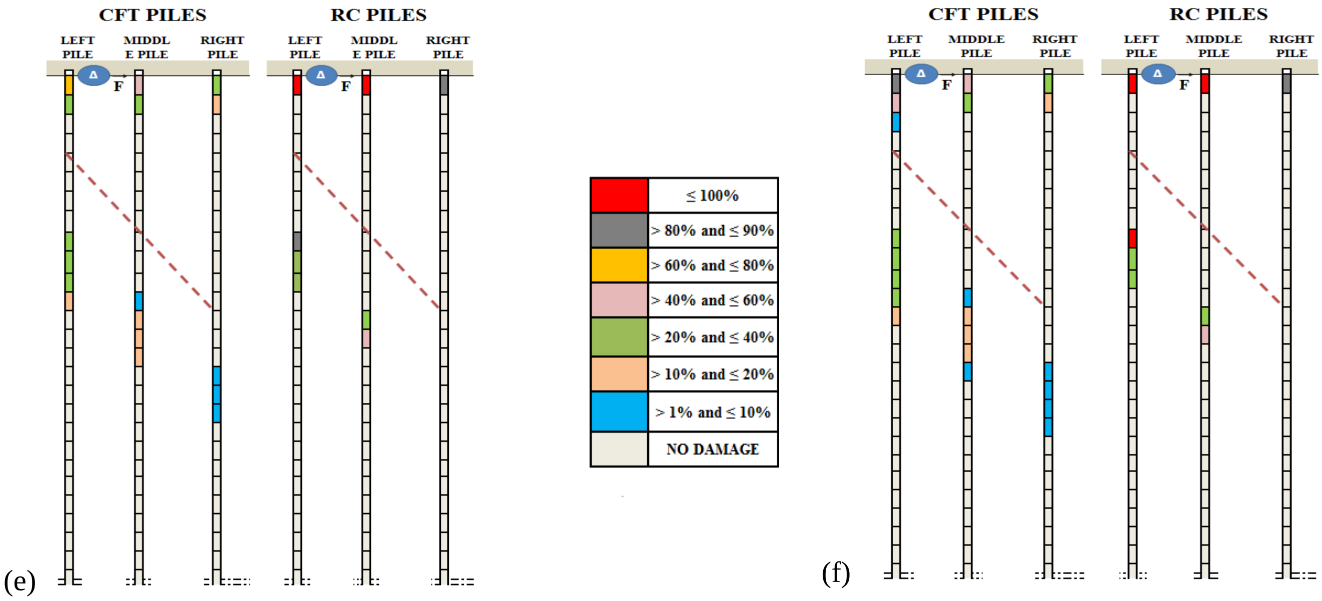

Figure 11: Damage pattern of CFT and RC piles under cyclic lateral loading condition for: (a) global displacement ductility 1u$_y$ (first cycle); (b) global ductility 1u$_y$ (second cycle); (c) global ductility 3u$_y$ (first cycle); (d) global ductility 3u$_y$ (second cycle); (e) global ductility 6u$_y$ (first cycle); and (f) global ductility 6u$_y$ (second cycle)

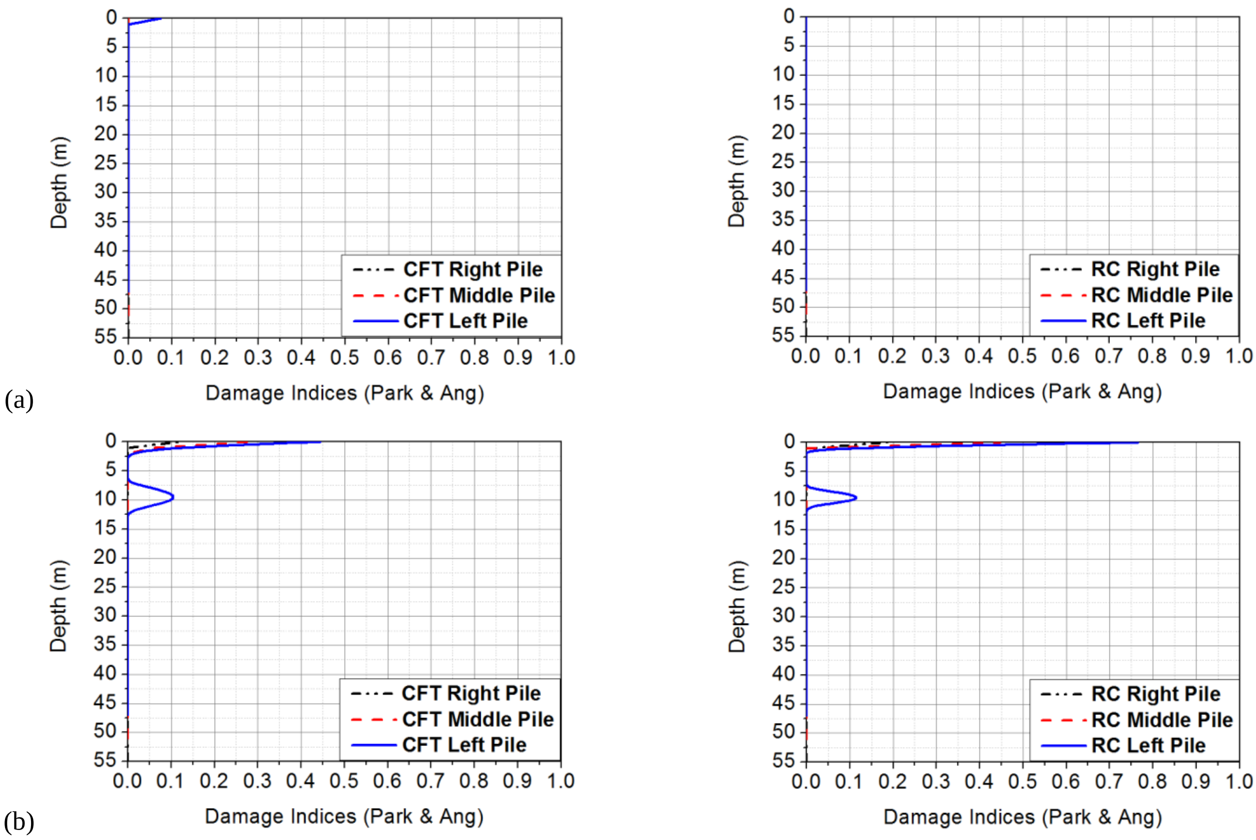

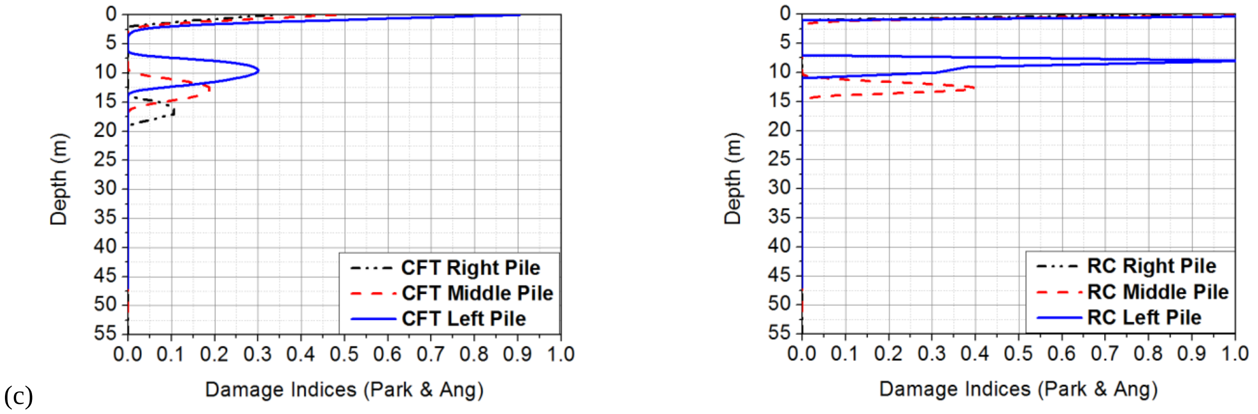

Figure 12: Damage index versus depth for CFT and RC piles under cyclic loading for: (a) global displacement ductility $1u_y$ (second cycle; (b) global ductility $3u_y$ (second cycle); and (c) global ductility $6u_y$ (second cycle)

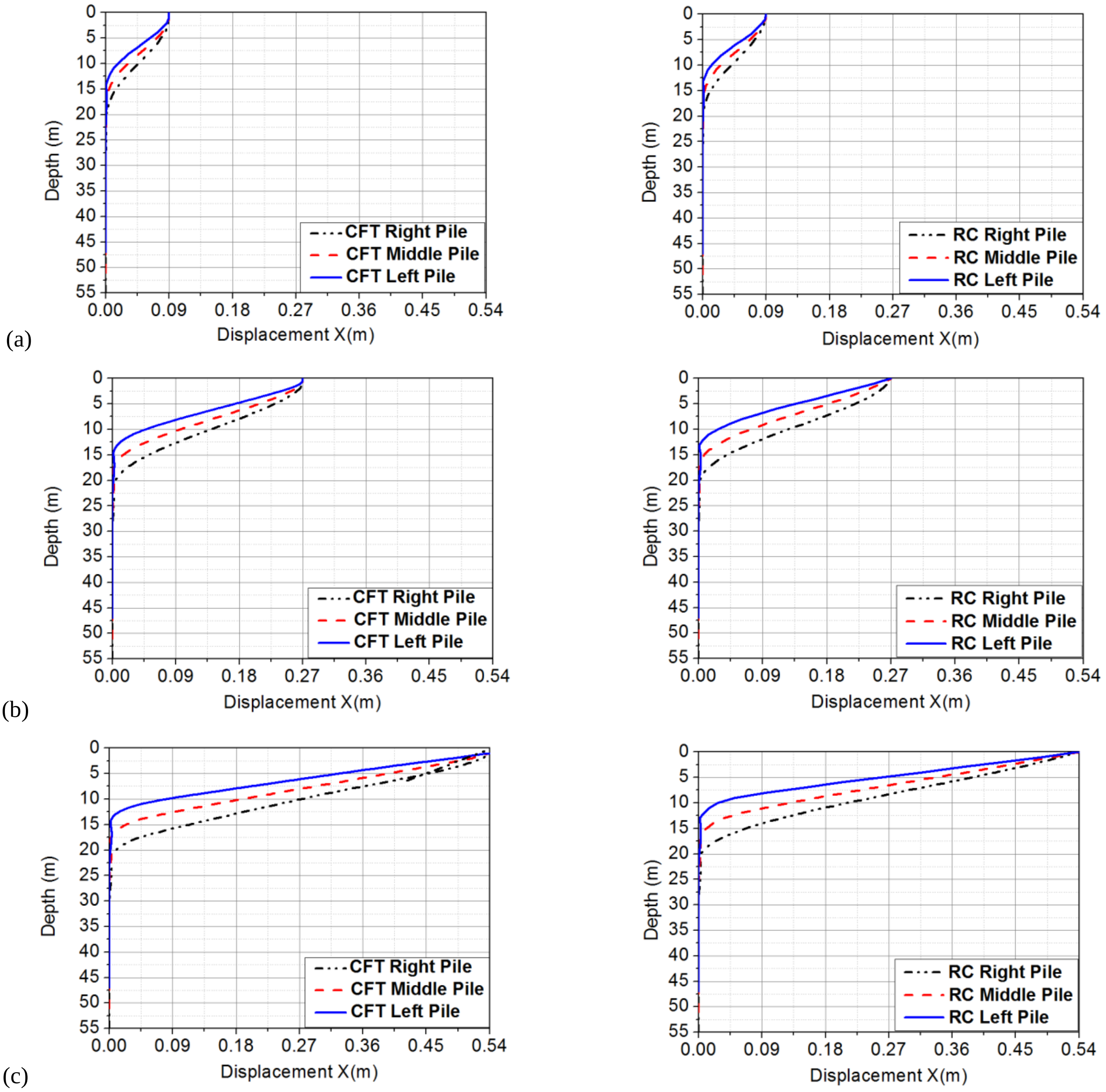

Figure 13: Displacement profile of CFT and RC piles under cyclic loading for: (a) global displacement ductility $1u_y$ (second cycle; (b) global ductility $3u_y$ (second cycle); and (c) global ductility $6u_y$ (second cycle)

According to Figs 11 and 12, it is observed that the most damage-prone area in piles is focused on the pile-heads which absorb a significant amount of input energy. Damage also appears in the part of the piles embedded into the upper layers of the soil stratigraphy up to a maximum soil depth equal to 8.5 m (i.e., 12.5 m depth minus 4 m free length of the left pile), as shown in Fig. 12c. This is likely to be related to the lateral stiffness contrast in the soil deposit that takes place at this location from loose sand to medium dense sand (Table 1). There are also some cases where damages appear only in the CFT piles, and more specifically in the upper soil layers of the right pile (Fig. 12c), but these are very small values. The damaged area of the CFT pile tends to be wider reaching lower values than the corresponding damaged area of RC piles for which an intense knee-shaped damage distribution with greater peaks is observed. The inelastic deformations appear to be more uniform and proportionally distributed in CFT piles than in RC piles which reduces the concentration of damage in the former. Research works [27, 28] on this topic have demonstrated that kinematic bending moments can be responsible for pile damage especially in the case of high stiffness discontinuity with multiple layered soils. In general, it is obvious that while the damage areas of both CFT and RC piles are mainly developed in the same regions of the pile-foundation system, CFT piles exhibit a lower damage than that of RC piles by 38% on average.

Figure 13 shows the displacement profile of CFT and RC piles for a wide range of displacements. According to this figure, the displacement profile of CFT piles tends to be the same as in RC piles for all cases. However, the left RC pile reaches similar maximum displacements with the middle RC pile. This phenomenon is more intense at high levels of global inelasticity (i.e., $3u_y$ and $6u_y$), and particularly when the left pile has reached high levels of damage. For the left pile a full lateral constraint can be seen in a depth more than 11 m (i.e., measured from the free soil surface), for the middle pile more than 12 m, while for the right pile more than 13 m. These depths are equal to 2.75, 1.50 and 0.92 times the free pile's length, repetitively. Moreover, based on the research study of Gajan and Kutter [64], a foundation system is more flexible when the moment-to-shear ratio is large leading to energy dissipation through soil layers and suffering less, whereas the system absorbs more energy for low moment-to-shear ratios. It can be concluded, therefore, that the left piles tend to exhibit greater damages while a large part of the input energy is absorbed by the upper more flexible than the deep soil layers. On the other hand, the middle and left pile tend to reach greater displacements with the corresponding upper soil layers to absorb less input energy. Based on the results, the damage in the left RC pile at the location of the head exceeds the value of 1.0 during the first cycle of global displacement ductility $6u_y$, while it reaches the value of 0.9 in a depth of 6 m from the free soil surface, thus indicating a collapse scenario (Fig. 12). For the CFT pile-head, the damage exceeds the value of 1.0 during the second cycle of global displacement ductility $6u_y$, but the damage of the pile within the soil is not greater than 0.25.

6. SEISMIC ANALYSES OF THE SOIL-PILE FOUNDATION SYSTEMS

In this section, a comparison between circular CFT and RC piles under seismic actions is conducted. The examined soil-pile foundation models are analyzed to a set of seismic events using Ruaumoko program [50]. As shown in Fig. 14, an ensemble of 7 ordinary (far-field type) ground motions recorded at soils with average shear wave velocity $v_{s,30}$ in the range between 360 and 800 m/s [classified according to EC8 [65] as soil type B] are selected from the NGA database [66] and are employed for the nonlinear time history analyses of this study. Another constraint on the selection of the earthquakes is that their geometric average spectrum is as near as possible to the

EC8 [65] elastic spectrum for ground acceleration α_{gR} = 0.36g in the range of periods between of $0.2T_1$ to $2T_1$, where T_1 is the fundamental natural period of the structure. The natural period of the present structure is nearly 1.50 seconds. Table 5 lists the seven ground motions considered here including their station and code names along with the scale factors (SF).

The pile-foundation systems are analyzed for two levels of seismic intensity. These are: (a) the reference seismic action associated with the design-basis earthquake (i.e., life safety performance level), (b) and the maximum considering earthquake (i.e., near collapse performance level). EC8 [65] gives no recommendation for the near collapse level, however, a very rare or maximum considered earthquake, which has values of the mean return period in the order of 1000 to 2500 years, can be considered. In this study, the design-basis earthquake events are further scaled by 1.70 times to account for the major event having a return period of 2,475 years. This scale factor was calculated by using the formula for the importance factor γ_I of EC8 [65] considering as a reference seismic action the one associated with return period 475 years (i.e., design-basis earthquake) based on which the ground motions listed in Table 4 were selected.

Table 5: Seismic input data of selected seismic events based on the reference seismic action [65]

Seismic events	Station	Mag	Code Name	$SF_{DBE}^{\dagger}$	SF_{MCE}^{*}	Direction
Chi-Chi, Taiwan	CHY029	7.62	RSN-1198	1.58	2.69	Horizontal component 1
Landers, USA	Joshua Tree	7.28	RSN-867	1.60	2.72	
Northridge, USA	Castaic – old Ridge Route	6.69	RSN-963	0.93	1.58	
Chi-Chi, Taiwan	CHY035	7.62	RSN-1202	1.30	2.21	
Cape Mendocino, USA	Ferndale Fire Station	7.01	RSN-3748	1.05	1.78	
Chuetsu-oki, Japan	Yoshikawaku Joetsu City	6.80	RSN-4850	1.48	2.50	
Iwate, Japan	Kurihara City	6.90	RSN-5818	1.12	1.90	

† Scale factor of the design-basis earthquake; *Scale factor of the maximum considering earthquake

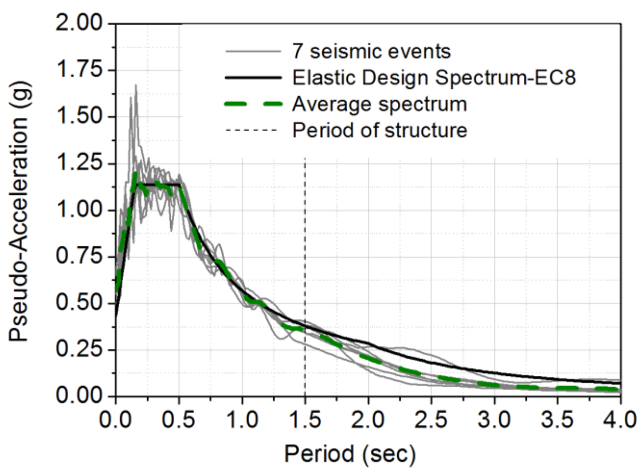

Figure 14: Acceleration response spectra of 7 seismic motions for soil class B compatible with EC8 [65]

Figures 15a and 15b depict the maximum and the average damage values as obtained from the time-history analyses for the design-basis and major seismic event, respectively. The structural damage was found to be greater on

RC pile-heads compared to CFT ones, while in some cases damage is twice. The whole RC structure exhibited a 30% and 53% greater damage than the CFT structure for the design-basis and major seismic event, respectively. In general, the damage becomes greater for the left pile-heads due to the small moment-to-shear ration and large rotation. For the major seismic event, both left and middle pile-heads of the RC structure have reached a maximum damage index close to 1.0 indicating the possibility of collapse. On the contrary, in CFT structure the middle and right pile-head reached a maximum damage index below 0.4 while the damage of the more vulnerable left pile-head has slightly exceeded 0.6.

Figures 16 and 17 analyze the seismic behaviour of the two soil-pile foundation systems illustrating the damage distribution of the most damage-prone areas, and the maximum displacement and damage index profiles of the whole system for a representative earthquake. More specifically, Fig. 16 discusses on results as obtained by analyzing the system under the Iwate ground motion using SF_{DBE} of Table 5, while Fig. 17 discusses on the same results as obtained by using SF_{MCE} for the same ground motion. As it was indicated in cyclic analysis results, damages tend to reach greater values in the pile-heads, while the part of the pile embedded into the upper soil layers exhibiting lower values. The soil dissipates an amount of the seismic energy, thus reducing the damage on the piles. Overall, a better seismic behaviour is observed for the CFT soil-pile foundation system which tends to dissipate the input energy more stably and uniformly allowing for some yielding within the upper layers of soil for the design-basis event. On the contrary, the RC soil-pile foundation system accumulates damage mainly in the pile-heads which is prompted by the pinching and deteriorating behaviour of the RC members. As the seismic input energy increases, damages are also observed for the RC piles in the region of the upper soil layers which appears to be another energy dissipating region after the pile-heads. In terms of displacements, both systems exhibit a very similar displacement profile with the CFT system reaching slightly higher values along the height of the piles and a smaller displacement on the pile-heads which is likely to be related to the more uniform distribution of the inelasticity within the system.

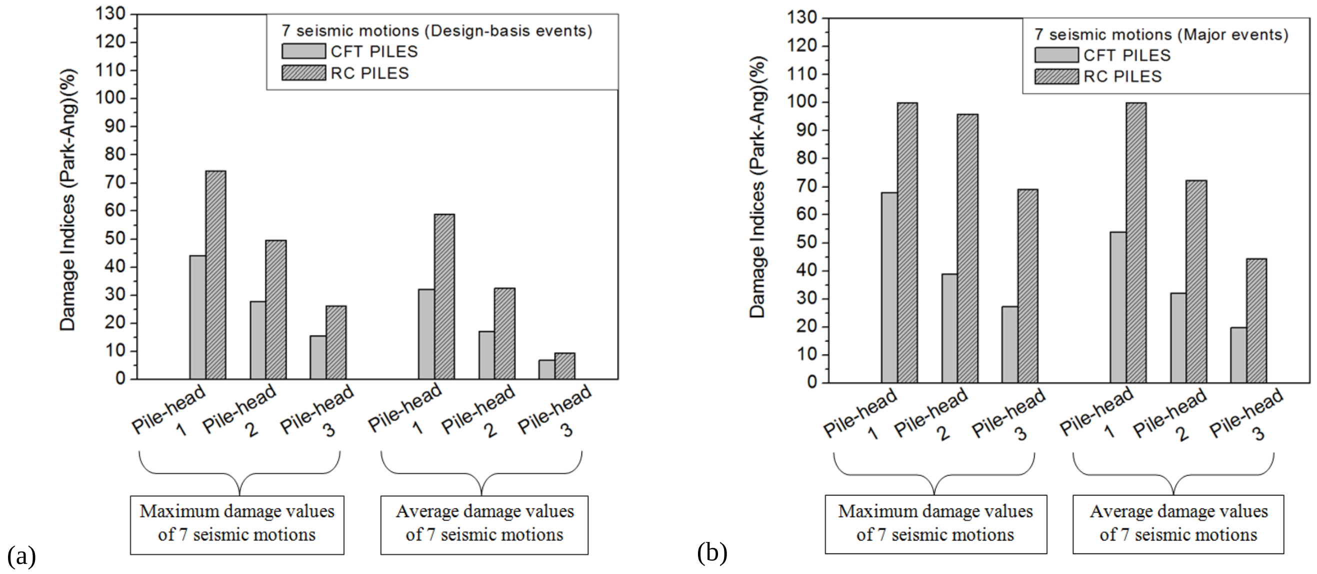

Figure 15: Average and maximum values of damage index for the CFT and RC piles under the 7 ground motions scaled to: (a) design-basis seismic event; and (b) maximum considering seismic event

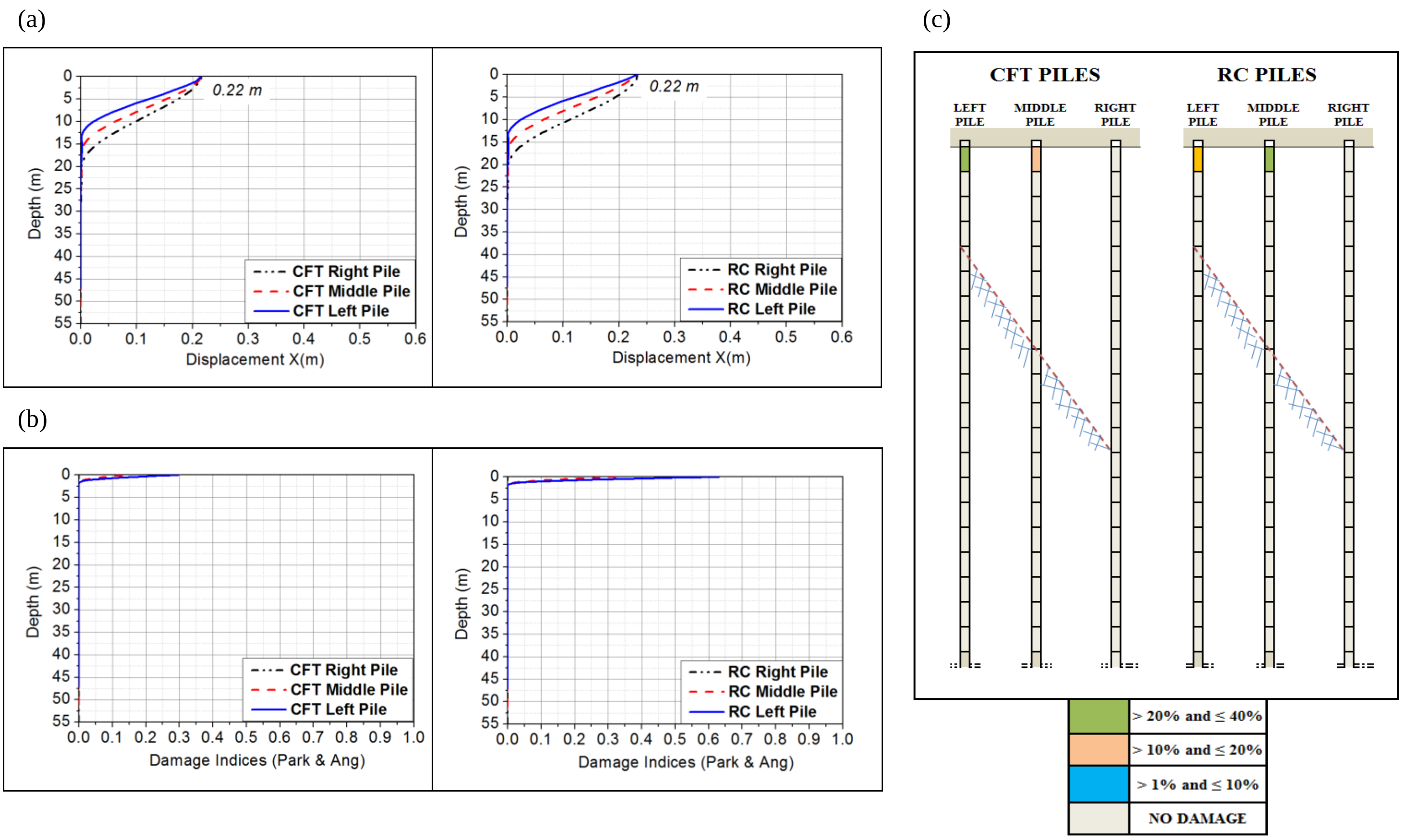

Figure 16: Comparison between CFT and RC soil-pile foundation system for Iwate seismic motion with SF_{DBE} = 1.12: (a) Displacement profile; (b) damage index profile; and (c) distribution of the damage

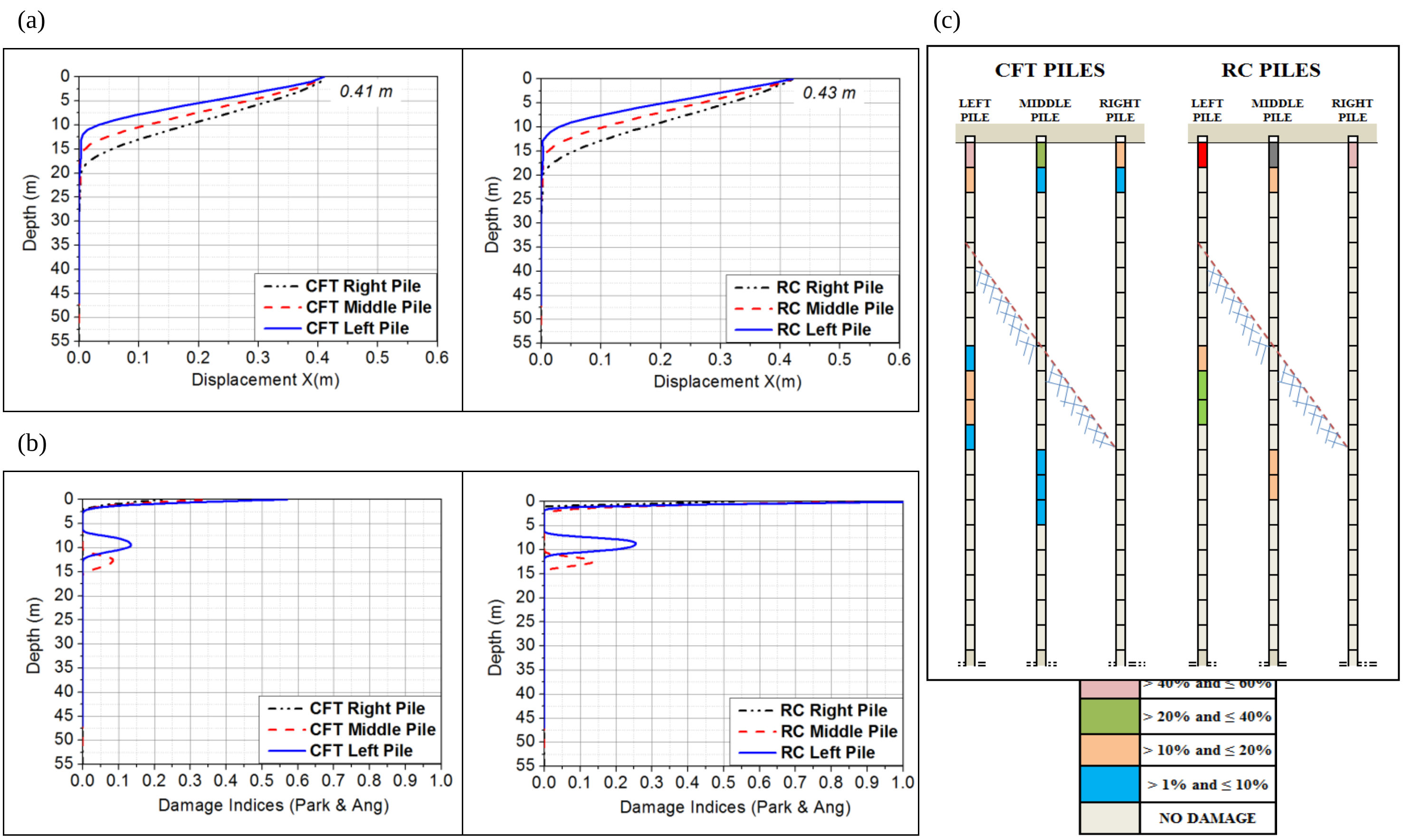

Figure 17: Comparison between CFT and RC soil-pile foundation system for Iwate seismic motion with SF_{MCE} = 1.90: (a) Displacement profile; (b) damage index profile; and (c) distribution of the damage

In this last section, Fig. 18 and Fig. 19 present the hysteretic behaviour of the three pile-heads in terms of normalized moment and displacement ductility for the seismic events of Cape Mendocino and Iwate, respectively, scaled by the factors of Table 5. In general, CFT piles provide a more stable and fatter hysteretic loop while in RC piles there is a strong pinching and deteriorating behavior that result in slightly larger inelastic displacements. Nevertheless, there are also cases where CFT piles start dissipating energy earlier than the RC piles which behave almost elastically. This can be seen in Fig. 19a for the middle and right piles. An evenly distribution of the energy dissipation helps the system to avoid accumulation of damage in a specific region. Fig. 19b clearly shows that the middle and right RC pile-heads suddenly enter the deterioration behaviour reaching greater inelastic displacements than the CFT pile-heads, while the left pile-head has almost lost the 50% of its flexural strength.

Accordingly, Fig. 20 and Fig. 21 present the displacement time histories of each pile-head for the same seismic events as in Figs 18 and 19. It can be seen that residual displacements appear in the soil-pile foundation system after experiencing the major event. For instance, a residual displacement of $0.50u_y$ and $0.25u_y$ was observed in RC left and middle pile, respectively, for the Cape Mendocino seismic event, while half residual displacements were observed in CFT piles. Residual displacements were also observed in RC piles for the Iwate seismic event, while no residual displacement were observed in CFT piles for this seismic event.

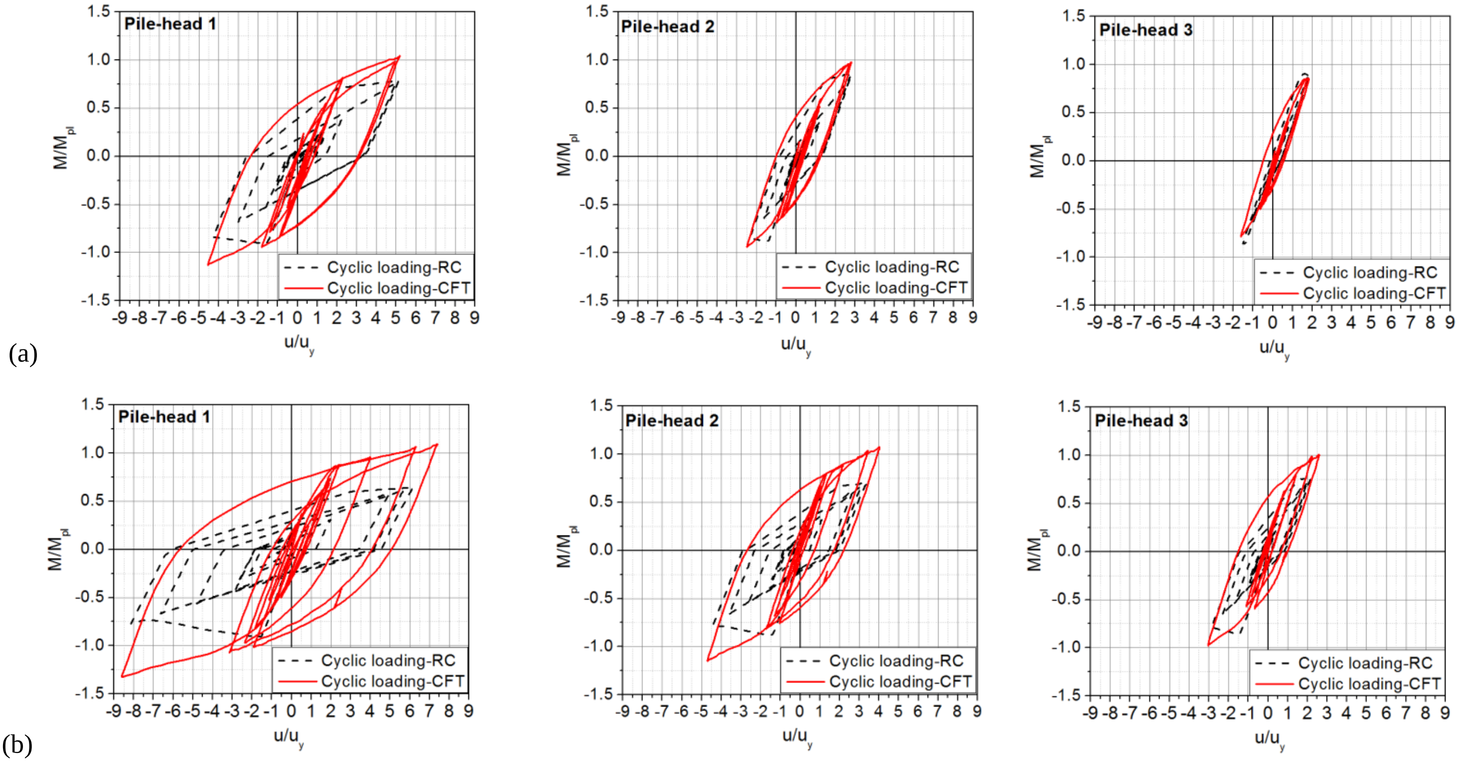

Figure 18: Comparison between hysteretic behaviour of CFT and RC pile-heads for the Cape Mendocino seismic motion: (a) $SF_{DBE} = 1.05$, (b) $SF_{MCE} = 1.75$

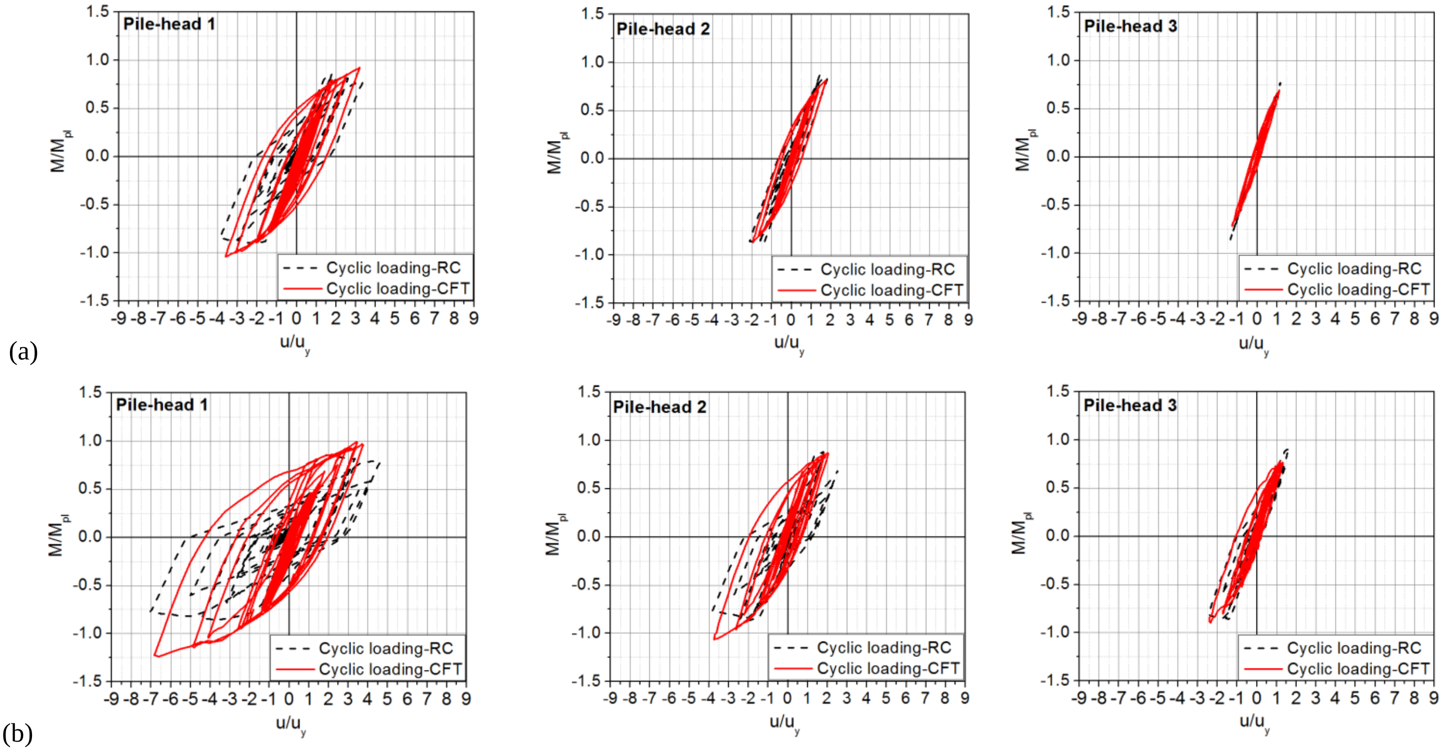

Figure 19: Comparison between hysteretic behaviour of CFT and RC pile-heads for the Iwate seismic motion: (a) $SF_{DBE} = 1.12$, (b) $SF_{MCE} = 1.90$

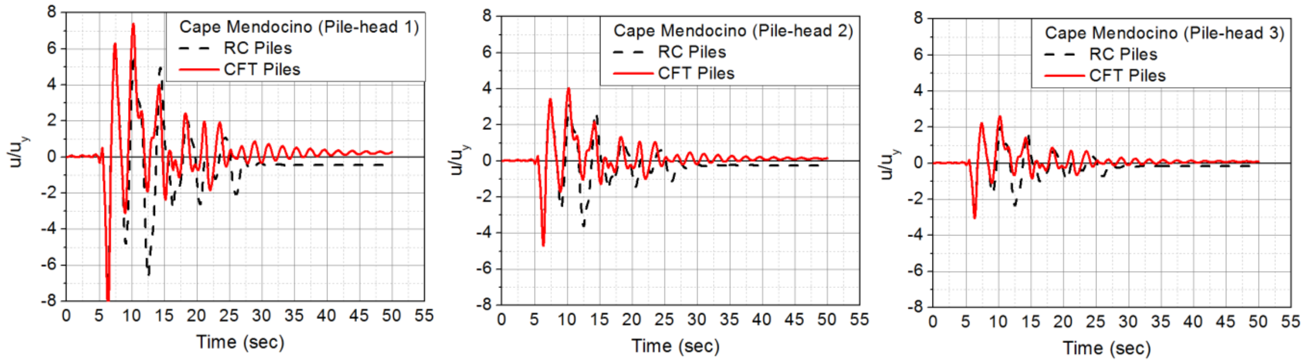

Figure 20: Comparison between displacement history of CFT and RC pile-heads for the major event of Mendocino seismic event ($SF_{MCE} = 1.75$)

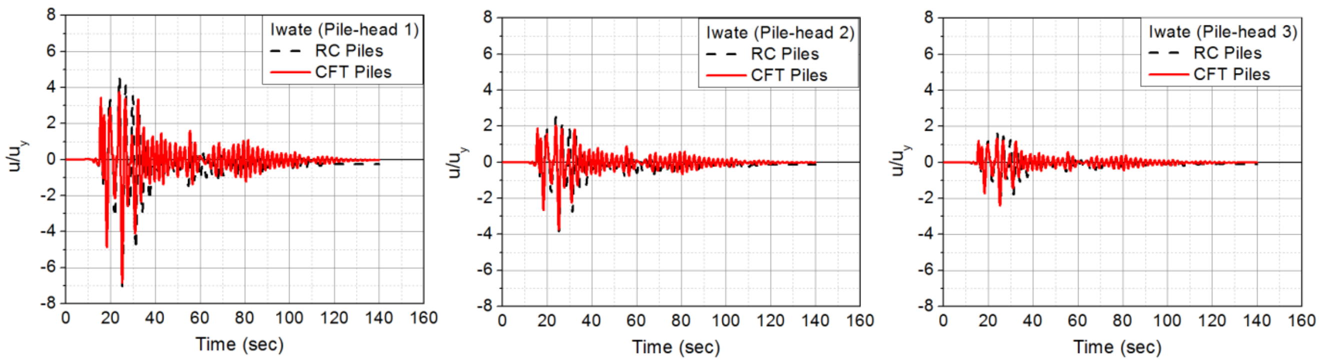

Figure 21: Comparison between displacement history of CFT and RC pile-heads for the major event of Iwate seismic event ($SF_{MCE} = 1.90$)

6. CONCLUSIONS

This study investigated the nonlinear response of composite steel-concrete soil-pile foundation systems subjected to lateral monotonic, cyclic and earthquake loads. For seismic analysis, two levels of seismic intensity were considered, i.e., the design basis earthquake (design-basis event) and the maximum occurring earthquake (major event). The mechanical behaviour for both soil and pile was simulated with the aid of concentrated plasticity models, while the soil-pile interaction was considered using the solution of p-y modelling technique. In addition to composite foundation, a reinforced concrete (RC) system was analyzed for comparison. The following findings and conclusions can be drawn:

1. The proposed analytical method can reliably describe the monotonic lateral and cyclic inelastic responses of soil-pile foundation systems for various geometrical and material properties both for the piles and the soil. The stiffness and strength have been traced with good accuracy. Although its simplicity, the developed p-y modeling can account for soil degradation effects making possible the simulation of the soil's cyclic behaviour.
2. The cyclic behaviour of CFT pile-heads exhibited a high hardening and stability. In RC pile-heads, the monotonic response is always higher than the peak values of the cyclic response due to strength degradation and pinching phenomena, particularly at large inelastic levels (global displacement ductility > $3u_y$). A cyclic strength reduction nearly 25~30% of the original strength of the monotonic non-degraded response was observed.
3. The most damage-prone area in piles is focused on the pile-heads which absorb a significant amount of input energy. Damage also appears in the part of the piles embedded into the upper layers of the soil stratigraphy up to a maximum soil depth equal to 8.5 m. The damaged area of the CFT pile tends to be wider reaching lower values than the corresponding damaged area of RC piles for which an intense knee-shaped damage distribution with greater peaks is observed.
4. Based on the cyclic analyses, the damage in the left RC pile at the location of the head exceeds the value of 1.0 during the first cycle of global displacement ductility $6u_y$, while it reaches the value of 0.9 in a soil depth of 6 m indicating a collapse scenario. For the CFT pile-head, the damage exceeds the value of 1.0 during the second cycle of global displacement ductility $6u_y$, but the damage of the pile within the soil is not greater than 0.25.
5. Overall, a better seismic behaviour is observed for the CFT soil-pile foundation system which tends to dissipate the input energy more stably and uniformly allowing for some yielding within the upper layers of soil for the design-basis seismic event. In terms of displacements, both systems exhibited a very similar displacement profile with the CFT system reaching slightly higher values along the height of the piles and a smaller displacement on the pile-heads which is likely to be related to the more uniform distribution of the inelasticity within the system.
6. Seismic damage was found to be greater on RC pile-heads compared to CFT ones, while in some cases damage is twice. The whole RC pile-foundation system exhibited a 30% and 53% greater damage than the CFT system for the design-basis and major seismic intensity, respectively. For the major event, both left and middle pile-heads of the RC system reached a maximum damage index close to 1.0.

7. CFT piles provide a more stable and fatter hysteretic behaviour while in RC piles there is a strong pinching and deteriorating behaviour (up to 50% flexural strength reduction) resulting in larger inelastic displacements. Residual displacements appeared in the soil-pile foundation system after experiencing the major seismic event. A residual displacement up to $0.50u_y$ was observed in RC piles with the CFT piles to experience half residual displacements. There were some cases with no residual displacements for the CFT system.

REFERENCES

[1] Bhattacharya S, Goda K (2013). Probabilistic buckling analysis of axially loaded piles in liquefiable soils. Soil Dynamics and Earthquake Engineering; 45: 13-24.

[2] Wei X, Wang Q, Wang J. Damage patterns and failure mechanism of bridge pile foundation under earthquake: Proceedings of the 14th World Conference on Earthquake Engineering, October 12-17, 2008, Beijing, China.

[3] Stacul S, Squeglia N (2018) KIN SP: A boundary element method based code for single pile kinematic bending in layered soil. Journal of Rock Mechanics and Geotechnical Engineering; 10(1): 176-187.

[4] Tokimatsu K, Hiroshi O.-O, Satake K, Shamoto Y, Asaka Y. (1997). Failure and deformation modes of piles due to liquefaction-induced lateral spreading in the 1995 Hyogoken-Nambu earthquake. Journal of Structural and Construction Engineering-AIJ (Japan); 5 (495): 95-100.

[5] Ishihara K (1997). Terzaghi oration: geotechnical aspects of the 1995 Kobe earthquake. Proceedings of 14th International Conference on Soil Mechanics and Foundation Engineering, Hamburg; (4): 2047–2073.

[6] Bhattacharya S, Madabhushi SPG (2008). A critical review of methods for pile design in seismically liquefiable soils. Bulletin of Earthquake Engineering; 6: 407-46.

[7] Zyka K, Mohajerani A (2016). Composite piles: A review. Construction and Building Materials; 107: 394-410.

[8] API (2000). Recommended practice for planning, designing and constructing fixed offshore platforms – working stress design. American Petroleum Institute.

[9] Elchalakani M, Zhao XL, Grzebieta R (2004). Concrete-filled steel circular tubes subjected to constant amplitude cyclic pure bending. Engineering Structures 26: 2125-2135.

[10] Zhao XL, Han LH, Lu H (2010). Concrete-filled tubular members and connections. Spon Press, New York.

[11] Serras DN, Skalomenos KA, Hatzigeorgiou GD, Beskos DE (2016). Modeling of circular concrete-filled steel tubes subjected to cyclic lateral loading. Structures Journal; 8(1): 75-93.

[12] Serras DN, Skalomenos KA, Hatzigeorgiou GD, Beskos DE (2017). Inelastic behavior of circular concrete-filled steel tubes: Monotonic vs. cyclic response. Bulletin of Earthquake Engineering; 15: 5413-5434.

[13] Skalomenos KA, Hatzigeorgiou GD, Beskos DE (2018). Seismic analysis and design of composite steel/concrete-filled steel tubular columns. In: Pitilakis K. (Eds.) Recent Advances in Earthquake Engineering in Europe. ECEE. Geotechnical, Geological and Earthquake Engineering-Springer, Cham; Vol. 46: pp. 387-411.

[14] Skalomenos KA, Hatzigeorgiou GD, Beskos DE (2015a), Seismic behavior of composite steel/concrete MRFs: deformation assessment and behavior factors. Bulletin of Earthquake Engineering; 13(12): 3871-3896.

[15] Skalomenos KA, Hatzigeorgiou GD, Beskos DE (2015b), Application of the hybrid force/displacement (HFD) seismic design method to composite steel/concrete plane frames. Journal of Constructional Steel Research, 115: 179-190.

[16] Skalomenos KA, Hatzigeorgiou GD, Beskos DE (2014). Parameter identification of three hysteretic models for the simulation of the response of CFT columns to cyclic loading. Engineering Structures; 61: 44-60.

[17] Skalomenos KA, Hayashi K, Nishi R, Inamasu H, Nakashima M (2016). Experimental behavior of concrete-filled steel tube columns using ultrahigh-strength steel. Journal of Structural Engineering; 142(9): 04016057

[18] Hajjar JF (2002). Composite Steel and Concrete Structural Systems for Seismic Engineering. Journal of Constructional Steel Research; 58: 703-728.

[19] Varma AH, Ricles JM, Sause R, Lu LW (2002). Experimental Behavior of High Strength Square Concrete-Filled Steel Tube Columns. Journal of Structural Engineering of ASCE; 128(3): 309-318.

[20] Herrera RA, Ricles JM, Sause R (2008). Seismic Performance Evaluation of a Large-Scale Composite MRF Using Pseudodynamic Testing. Journal of Structural Engineering of ASCE; 134(2): 279-288.

[21] Denavit MD, Hajjar JF, Perea T, Leon TR (2016). Stability Analysis and Design of Composite Structures. Journal of Structural Engineering; 142(3): doi/abs/10.1061/(ASCE)ST.1943-541X.0001434

[22] Silva A, Jiang Y, Macedo L, Castro JM, Monteiro R, Silvestre N (2016). Seismic performance of composite moment-resisting frames achieved with sustainable CFST members; Frontiers of Structural and Civil Engineering; 10: 332-332.

[23] Chen J, Chan TM, Su RKL, Castro JM (2019). Experimental assessment of the cyclic behaviour of concrete-filled steel tubular beam-columns with octagonal sections. Engineering Structures; 180: 544-560.

[24] Lai MH and Ho JCM (2014). Confinement effect of ring-confined concrete-filled-steel-tube columns under uni-axial load. Engineering Structures; 67: 123-141.

[25] Lai MH and Ho JCM (2016). A theoretical axial stress-strain model for circular concrete-filled-steel-tube columns. Engineering Structures; 125: 124-143.

[26] Wang QL, Shao YB (2015). Flexural performance of circular concrete filled CFRP-steel tubes, Advanced Steel Construction; 11(2): 127–149.

[27] Di Laora R, Mandolini A, Mylonakis G (2012). Insight on kinematic bending of flexible piles in layered soil. Soil Dynamics and Earthquake Engineering; 43: 309-322.

[28] Di Laora R, Mylonakis G, Mandolini A (2013). Pile-head kinematic bending in layered soil. Earthquake Engineering & Structural Dynamics; 42(3): 319-337.

[29] Li Q, Yang ZJ (2017). P-Y approach for laterally loaded piles in frozen silt. Journal of Geotechnical and Geoenvironmental Engineering of ASCE; 143(5): 04017001.

[30] Li J, Chengzhi W (2016). Bearing properties of large-diameter embedded rock-socketed pile with steel tube in frame wharf. Electronic Journal of Geotechnical Engineering; 21(10): 3797-3813.

[31] Yunxiu D, Zhongju F, Haibo H, Jingbin H, Qilang Z, Fuchun W (2020). The Horizontal Bearing Capacity of Composite Concrete-Filled Steel Tube Piles. Advances in Civil Engineering, vol. 2020, Article ID 3241602, 15 pages, 2020. https://doi.org/10.1155/2020/3241602

[32] Li X, Xiao Y, Xu Y-M, Lu J, Ding D-B, Zhou T (2020). Structural behaviour of double-CFT-pile foundations under cyclic loads, Soil Dynamics and Earthquake Engineering; 128: 105863

[33] Wakai A, Gose S and Ugai K (1999). 3-D elasto-plastic finite element analyses of pile foundations subjected to lateral loading. Soils and Foundations; 39(1): 97-111.

[34] Rollins KM, Peterson KT, Weaver TJ (1998). Lateral load behavior of full-scale pile group in clay. Journal of Geotechnical Engineering of ASCE; 124(6): 468-478.

[35] Tuladhar R, Maki T, Mutsuyoshi H (2007). Cyclic Behavior of Laterally Loaded Concrete Piles Embedded into Cohesive Soil. Earthquake Engineering and Structural Dynamics, 37(1): 43-59.

[36] Brown DA, Shie CF (1990). Numerical experiments into group effects on the response of piles to lateral loading. Computers and Geotechnics; 10: 211-230.

[37] Trochanis AM, Bielak J, Christiano P (1991). Three-dimensional nonlinear study of piles. Journal of Geotechnical Engineering of ASCE; 117(3): 429-447.

[38] Brown DA, Shie CF (1990). Numerical experiments into group effects on the response of piles to lateral loading. Computers and Geotechnics; 10(3): 211-230.

[39] Adachi T, Kimura M, Zhang F (1994). Analyses on ultimate behavior of lateral loading cast-in-place concrete piles by 3-dimensional elasto-plastic FEM: In Proceedings of the 8th International Conference on Computer Methods and Advances in Geomechanics. Morgantown, USA; 2279-2284.

[40] Zhang F, Kimura M, Nakai T, Hoshikawa T (2000). Mechanical behavior of pile foundations subjected to cyclic lateral loading up to the ultimate state. Soils and Foundations; 40(5): 1-17.

[41] Elgamal A, Yan L, Yang Z, Conte J (2008). Three-dimensional seismic response of Humboldt Bay bridge–foundation–ground system. Journal of Structural Engineering of ASCE; 134(7): 1165–1176.

[42] Jeremic B, Jie G, Preisig M, Tafazzoli N (2009). Time domain simulation of soil–foundation–structure interaction in nonuniform soils. Earthquake Engineering and Structural Dynamics; 38(5): 699–718.

[43] Mosher RL, Dawkins WP (2000). Theoretical manual for pile foundations. US Army Corps of Engineers, Oklahoma State University, USA.

[44] El Naggar MH, Bentley KJ (2000). Dynamic analysis for laterally loaded piles and dynamic p-y curves. Canadian Geotechnical Journal; 37(6): doi.org/10.1139/t00-058

[45] Zhang XL, Zhao Jj, Xu Cs (2020). A method for p-y curve based on Vesic expansion theory. Soil Dynamics and Earthquake Engineering; 137: 106291.

[46] Hyunsung L, Sangseom J (2018). Simplified p-y curves under dynamic loading in dry sand. Soil Dynamics and Earthquake Engineering; 113: 101-11.

[47] Aygun B, Dueñas-Osorio L, Padgett JE, DesRoches R (2011). Efficient longitudinal seismic fragility assessment of a multispan continuous steel bridge on liquefiable soils. Journal of Bridge Engineering of ASCE; 16(1): 93–107.

[48] Wang Z, Dueñas-Osorio L, Padgett JE (2013). Seismic response of a bridge–soil–foundation system under the combined effect of vertical and horizontal ground motions. Earthquake Engineering and Structural Dynamics; 42 (4): 545–564.

[49] Galindo RA, Lara A, Melentijevic S (2019). Hysteresis model for dynamic load under large strains. International Journal of Geomechanics-ASCE; 19(6): doi/10.1061/(ASCE)GM.1943-5622.0001428.

[50] Carr AJ (2008). Inelastic Time-History Analysis of Two-Dimensional Framed Structures. Department of Civil Engineering, University of Canterbury, New Zealand.

[51] Panagaki S (2017). Investigation of seismic inelastic behavior of deep foundations, Master thesis, Hellenic Open University, Patras, Greece.

[52] Kamaris G, Skalomenos KA, Hatzigeorgiou GD, Beskos DE (2016). Seismic damage estimation of in-plane regular steel/concrete composite moment resisting frames. Engineering Structures; 115: 67-77.

[53] Hatzigeorgiou GD, Liolios AA (2010). Nonlinear behaviour of RC frames under repeated strong ground motions. Soil Dynamics and Earthquake Engineering; 30: 1010-1025.

[54] European Committee of Standardization. Eurocode 2 (2002): Design of concrete structures, Part 1: General rules and rules for buildings. CEN, Brussels, EN 1992-1-1.

[55] Penelis G, Kappos A (1997). Earthquake resistant concrete structures, 1st edition. CRC Press: London.

[56] Tuladhar R, Maki T, Mutsuyoshi H (2007). Cyclic behavior of laterally loaded concrete piles embedded into cohesive soil. Earthquake Engineering Structural Dynamics; 37(1): 43-59.

[57] Inai E, Mukai A, Kai M, Tokinoya H, Fukumoto T, Mori K (2004). Behavior of concrete-filled steel tube beam columns, Journal of Structural Engineering of ASCE; 130(2): 189-202.

[58] Han LH, Yang YF (2004). Cyclic performance of concrete-filled steel CHS columns under flexural loading. Journal of Construction Steel Research; 61: 423-452.

[59] Hoit MI, McVay M, Hays C, Andrade PW (1996). Nonlinear pile foundation analysis using Florida-Pier. Journal of Bridge Engineering – ASCE; 1(4): 135-142.

[60] Lin C., Han J., Bennett C. and Parsons R.L. (2016). Analysis of the laterally loaded piles in soft clay considering scour-hole dimensions, Ocean Engineering; 111: 461-470.

[61] Liolios A, Efthymiopoulos P, Mergoupis T, Rizavas V, Chalioris CE (2017). Reinforced concrete frames strengthened by tension- tie elements under cyclic loading: Experimental investigation. In: Papadrakakis, M. et al (eds.), Proceedings of COMPDYN 2017: Computational Methods in Structural Dynamics and Earthquake Engineering, paper C18197, 15-17 June 2017, Rhodes Island, Greece.

[62] Park YJ, Ang AHS (1985). Mechanistic seismic damage model for reinforced concrete. Journal Structural Engineering of ASCE; 111(4): 722-739.

[63] Park YJ, Ang AHS, Wen YK (1987). Damage limiting a seismic design of buildings. Earthquake Spectra; 3(1): 1-26.

[64] Gajan S, Kutter BL (2009). Effects of Moment-to-Shear Ratio on Combined Cyclic Load-Displacement Behavior of Shallow Foundations from Centrifuge Experiments. Journal of Geotechnical and Geoenvironmental Engineering of ASCE; 135(8): 1044-1055.

[65] European Committee of Standardization. Eurocode 8 (2004): Design of structures for earthquake resistance, Part 1: General rules, seismic actions and rules for buildings, EN 1998-1, Brussels.

[66] Ancheta TD, Darragh RB, Stewart JP, Seyhan E, Silva WJ, Chiou BS-J, Wooddell KE, Graves RW, Kottke AR, Boore DM, Kishida T, Donahue JL (2014). NGA-West2 database. Earthquake Spectra 30(3): 989-1005.